Internal mouth bar variability and preservation of interflood beds in low-accommodation proximal deltaic settings (Cretaceous Dakota Group, New Mexico, USA)

Anna E. van Yperen[1], Miquel Poyatos-Moré[1], John M. Holbrook[2], & Ivar Midtkandal[1]

[1]University of Oslo, Department of Geosciences, P.O. Box 1047 Blindern, 0316 Oslo, Norway

[2]Texas Christian University, Department of Geological Sciences, TCU Box 298830, Fort Worth, Texas 76129

Corresponding author: annavanyperen@gmail.com

Key words: low accommodation, mouth bar, delta, interflood beds, preservation, Dakota Group

ABSTRACT

Mouth bars are the fundamental architectural elements of proximal deltaic successions. Understanding their internal architecture and deciphering the relative impact and complex interaction of coastal processes (fluvial-, tide- and wave-dominated) is paramount to the interpretation of ancient deltaic successions. This is particularly challenging in low-accommodation systems, because they are commonly characterized by thin, condensed and top-truncated sections. In this study, we analyze the exhumed Cenomanian Mesa Rica Sandstone (Dakota Group, Western Interior Seaway, USA), which encompasses a fluvio-deltaic system covering a ~450 km profile oriented parallel to depositional-dip direction. The study targets the proximal deltaic expression of the system, with 22 sedimentary logs (total of 390 m) spatially correlated within a ~25 km2 study area at the rim of the Tucumcari Basin. Analysis of facies distributions, depositional architecture and spatial extent of stratigraphic surfaces reveals a 6–10-m-thick, sharp-based and sand-prone deltaic package, comprising several laterally-extensive (>800 m width) mouth bars. Composite erosional surfaces infilled with multi-story fluvial and marine-influenced channel deposits (12–20 m thick, 100–250 m wide) scour locally into the deltaic package. Based on differences in sedimentary structures, bed thicknesses, occurrence of interflood beds and bioturbation indexes, we distinguish four different subenvironments within single mouth bars. These range from mouth bar axis, off-axis, fringe to distal fringe deposits, and each reflect differences in hydraulic conditions as moving away from the main active feeding channel. The interpreted mouth bar components also show intra-mouth-bar variability in dominant process regime, with overall river dominance but local preservation of tide influence in the fringe and distal fringe components. Mouth bar deposits amalgamate to form an extensive sand-rich sheet body throughout the study area, in which interflood mudstone to very-fine grained sandstone beds are nearly absent. These features are interpreted to reflect successive

coalescence of mouth bars in a low accommodation / supply (A/S) setting. These conditions promoted channel avulsion/bifurcation and thus the potential reworking of previously deposited mouth bar fringe and distal fringe sediments, where tide influence tends to be better recorded. Results of this study evidence a common mixed nature and internal process-regime variability within mouth bar components. They also caution against the possible loss of preservation of subordinate processes (e.g. tidal indicators), and consequent underestimation of the true mixed influence in low-accommodation deltaic settings.

INTRODUCTION

Mouth bars are fundamental architectural elements of proximal deltaic successions. They form at the river mouth, where flows confined within a distributary channel expand and decelerate as they enter a standing body of water (Bates, 1953; Wright, 1977; Elliott, 1986). The plan-view, cross-sectional geometry and scale of mouth bars is controlled by the relative dominance of coastal processes, influencing their shape and typical aspect ratio (length: width) (e.g. Wright, 1977; Postma, 1990; Bhattacharya, 2006; Gani and Bhattacharya, 2007). Additionally, increased bedload and/or shallower receiving water depths result in broad mouth bar deposits, as enhanced effects of bed friction cause more rapid spatial expansion and deceleration of the river jet (Wright, 1977). Mouth bar depositional cycles consist of deposition, extension, avulsion and abandonment (Olariu and Bhattacharya, 2006). Numerical modeling suggest that individual mouth bars prograde until the water depth over the bar is equal to or less than 40% of the inlet depth, after which aggradation becomes dominant (Edmonds and Slingerland, 2007). This decreases distributary channel discharge and forces its bifurcation (Olariu and Bhattacharya, 2006; Edmonds and Slingerland, 2007) or avulsion (e.g. Bhattacharya, 2010). Both options lead to the initiation of new mouth bar deposition, and they are enhanced in high sediment supply and low accommodation conditions (Van Yperen et al., *in press JSR*).

Mouth bars consist of beds and bedsets that reflect flood and interflood deposition related to seasonal variations in flow conditions and sediment input (Dalrymple et al., 2015; Gugliotta et al., 2016a). Finer-grained facies (i.e., 'interflood beds') deposit during times of low energy between river flood periods, whereas 'river flood beds' are thicker and consist of coarser-grained facies deposited during times of high river discharge (Dalrymple et al., 2015; Gugliotta et al., 2016a). River flood beds are amalgamated towards the top and are dominant in the proximal part of mouth bars, whereas interflood beds occur predominantly at mouth bar fringes (Fig. 1) (Gugliotta et al., 2016a). If not obscured by bioturbation, and if deposition takes place within a tide-influenced zone, these interflood beds can show tidal rhythmites, double mud drapes, and/or bidirectional current ripples (Dalrymple et al., 2015, and references therein).

If a depositional system or zone experiences only weak tidal energy, tidal indicators have highest preservation potential in the interflood beds (e.g. Gugliotta et al., 2016b; Kurcinka et al., 2018). These interflood beds represent more time than the flood deposits (e.g. Miall, 2015).

Beds and bedsets within mouth bars represent basinward-accreting bar-front surfaces (e.g. Gani and Bhattacharya, 2007) emanating from a relatively fixed distributary channel mouth (Wellner et al., 2005). Individual mouth bars coalesce and stack compensationally to form mouth bar complexes (Fig. 2) (e.g. Wellner et al., 2005; Enge et al., 2010). Mouth bar complexes are related to the same progradation pulse (Ainsworth et al., 2016) and their distributary channel network is genetically linked (Wellner et al., 2005). Delta lobes consist of mouth bar complexes related to the same primary distributary feeder channel; new lobes form when the channel avulses or erodes through the delta lobe and initiates new, larger-scale mouth bar deposits outside the stranded lobe (Ainsworth et al., 2016). At both mouth bar complex and delta lobe scale, individual mouth bars typically become smaller and finer-grained as the distributary channel network progrades (Wellner et al., 2005). The amalgamation of mouth bars into mouth bar complexes and delta lobes is the building mechanism for deltas, and avulsion and/or bifurcation are the driving forces for their lateral development (Edmonds and Slingerland 2007).

Internal differentiation of individual mouth bars is executed but not common in ancient deltaic successions (e.g. Olariu and Bhattacharya, 2006; Gani and Bhattacharya, 2007; Enge et al., 2010; Jerrett et al., 2016; Fidolini and Ghinassi, 2016). In deep-water sedimentology it is common to differentiate submarine fan lobe deposits internally and distinguish lobe axis, off-axis, fringe and distal fringe sub-environments (e.g. Hodgson, 2009; Prélat et al., 2009; Hofstra et al., 2016; Spychala et al., 2017). A similar subdivision in ancient mouth bar deposits is uncommon but differentiation between axial and fringe deposits has been made (e.g. Jerrett et al., 2016; Fidolini and Ghinassi, 2016). Detailed work on modern deltas shows predictable grainsize and bedform trends within individual mouth bar deposits (e.g. Wellner et al., 2005). These are all consistent with an overall waning flow lithofacies association in all directions away from the central axis.

In this study, we analyze the proximal deltaic expression of the exhumed Cenomanian Mesa Rica Sandstone (Dakota Group, Western Interior Seaway, USA), with the aim to: i) describe and analyse the spatial distribution of sedimentary facies and stratigraphic architecture of its proximal deltaic expression; ii) distinguish and discuss different processes and deposits from internal mouth bar components; and iii) discuss the role of low-accommodation conditions in resulting deltaic geometries and preservation potential of interflood deposits.

GEOLOGICAL SETTING AND STRATIGRAPHIC FRAMEWORK

The Mesa Rica Sandstone (hereafter referred to as 'Mesa Rica') was deposited ~98-99 Ma during the Cenomanian (Scott et al., 2018) and is the oldest formation within the Dakota Group in Colorado and New Mexico (e.g. Holbrook and Wright Dunbar, 1992; Scott et al., 2004). The Dakota Group is among the eastward prograding sedimentary systems of the US Western Interior that were sourced from the Sevier fold-and-thrust belt (e.g. MacKenzie and Poole, 1962; Dickinson, 2018 and references herein, Van Yperen et al., *in press NMGS*). The latter formed during the Cordilleran orogeny, with subduction of the Farallon plate beneath the west coast of North America causing back-arc compression in the Late Jurassic (DeCelles, 2004). The Dakota Group also received minor sediment volumes from other smaller topographic highs (Kisucky, 1987; Holbrook and Wright Dunbar, 1992). The study area is located at the northwestern rim of the Tucumcari Basin (Fig. 3A), which formed during the late Carboniferous and early Permian as a tectonic element of the Ancestral Rocky Mountains (Broadhead, 2004).

An overall NW to SSE-directed depositional profile characterizes the Dakota Group in southeastern Colorado and northeastern New Mexico. The Dakota Group is further subdivided into the Mesa Rica, Pajarito (Dry Creek Canyon member in south-central Colorado and northeastern New Mexico) and Romeroville formations. These represent phases of predominantly fluvial, paralic, and fluvial deposition, respectively (Fig. 3B). Regional sequence boundary SB3.1 (Fig. 3B) forms the base of the Mesa Rica and relates to a late Albian – early Cenomanian forced-regression, which caused widespread erosion in southeast Colorado and northeast New Mexico (Holbrook and Wright Dunbar, 1992; Holbrook, 1996; Holbrook, 2001; Scott et al., 2004; Oboh-Ikuenobe et al., 2008). In east-central New Mexico, only the Mesa Rica and Pajarito formations are preserved, and the former can be in turn subdivided into the lower, middle, and upper Mesa Rica (Scott et al., 2004; Van Yperen et al., *in press NMGS*). This subdivision relates to depositional transgression-regression (T-R) cycles and record higher-frequency relative sea-level fluctuations in the Western Interior Seaway (e.g. Holbrook and Wright Dunbar 1992; Holbrook 1996; Scott et al., 2004; Oboh-Ikuenobe et al., 2008). In the Tucumcari Basin, the open marine Albian-Cenomanian Tucumcari Shale separates the fluvial Jurassic Morrison Formation from the fluvio-deltaic, Cretaceous Dakota Group (Fig. 3B) (e.g. Holbrook and Wright Dunbar 1992; Scott et al., 2004; Van Yperen et al., *in press JSR*). The Tucumcari Shale is locally underlain by estuarine deposits of the informally defined Cretaceous Campana Sandstone Bed (hereafter referred to as "Campana") (Holbrook et al., 1987; Holbrook and Wright Dunbar, 1992). This represents the sandy infill of local topographic lows, as the Late Jurassic landscape was progressively inundated during relative sea-level rise (Holbrook et al., 1987).

The lower Mesa Rica shows a change from fluvial to deltaic deposits at the northwestern rim of the Tucumcari Basin, which reflects the most proximal shallow-marine deposition within the Mesa Rica depositional system (Holbrook and Wright Dunbar, 1992; Van Yperen et al., *in press NMGS).* Upstream, time-equivalent fluvial strata record deposition of a >80 km-wide single-story channel sheet (e.g. Holbrook, 2001). Downstream, in the center of the Tucumcari Basin, coalesced mouth bars consistently overlain by sand-filled amalgamated distributary channels characterize the contemporaneous deltaic deposits (Van Yperen et al., *in press JSR*). The upper Mesa Rica represents a lower delta plain environment with fluvial distributary channel deposits (e.g. Scott et al., 2004; Holbrook et al., 2006; Van Yperen et al., *in press NMGS*) and an increased presence of marine-influenced distributary channel deposits towards the center of the basin (Van Yperen et al., *in press JSR).*

During the Cretaceous, the study area was located at ~35^0 N latitude, with a prevailing warm and humid climate (Chumakov et al., 1995).

METHODS AND DATA

The field study focused on the lower Mesa Rica, which is deltaic in the study area, because the main objective of this work is the recognition of internal architecture of ancient deltaic sandstone bodies. However, the upper Mesa Rica and the stratigraphic relationships with underlying and overlying strata are also briefly reported in the results below.

Stratigraphic sections were measured at 1:100 cm scale (18 logs) and 1:200 cm scale (4 sketch logs) within a **~**25 km^2 area, at the Trigg Ranch in San Miguel County, east-central New Mexico (Fig. 4). Sedimentary facies analysis was based on lithology, texture, sedimentary structures, and bioturbation assemblage and intensity. The latter was recorded using the 1–6 bioturbation index (BI) scheme of Taylor and Goldring (1993). UAV (unmanned aerial vehicle) imagery (shot with a Phantom 4 Pro ®)**,** photomontages, and field sketches are used to map sedimentary body geometries, lateral distributions, architectural elements and extension of key stratigraphic surfaces. These form the basis of a fence correlation diagram that correlates constructed depositional-dip (~6,5 km) and strike-oriented (**~**4 km) panels. Paleocurrent measurements (N=260) were obtained from cross-stratification and cross-lamination foresets.

FACIES ANALYSIS

The studied strata are divided into 13 facies (f1–13) based on observations of lithology, grain size, sedimentary structures, paleocurrents, bioturbation indices, and interpreted depositional processes

(Table 1, Figs. 5–9). We grouped the facies into nine facies associations (FA1–9) that reflect different environments of deposition, based on the combination of dominant sedimentary processes (facies), bioturbation intensity, and lateral and vertical facies relationships.

FA1 – Prodelta

Description - Gray, structureless muddy siltstone (f1, Table 1) found in sharp contact with overlying delta front deposits (FA2-FA5). FA1 thicknesses average 0.3–0.7 m (max. 2 m thick). Bioturbation indices are high (BI 4–5) and we identified *Thalassinoides, Phycosiphon, Planolites, Teichichnus, Chondrites,* and *Helminthopsis* (Fig. 7A). Macrofauna was not observed.

Interpretation - Deposition occurred below fair-weather wave base, in a low-energy setting beyond the influence of the river effluent (e.g. Wright and Coleman, 1973; Gani et al., 2009). The stratigraphic position of FA1 relates to the open marine Tucumcari Shale, with abundant macrofauna (e.g. *Texigrapheya, Peilina levicostata)* within the Tucumcari Basin (e.g. Scott, 1974; Holbrook and Wright Dunbar, 1992; Kues, 1997; Oboh-Ikuenobe et al., 2008). In the study area however, a shallower setting is inferred from the thin and silty appearance and lack of macrofauna indicative of open marine settings (e.g. Holbrook et al., 1987; Kisucky, 1987; Holbrook and White, 1998). The trace fossils indicate brackish to normal marine conditions (MacEachern and Bann, 2008).

FA2 – Mouth bar axis

Description – FA2 consists of two subsets: FA2.a consists of laterally-extensive sandstone beds with a tabular, sharp-bedded nature and display an alternation of f2 with f3, f4 and/or f5 (Fig. 8A, Table 1).Facies f2 consists of 10–30-cm-thick poorly-sorted, clast supported conglomerate beds with common (faint) stratification (Fig. 5A). Facies f3 consists predominantly of 30–50-cm-thick fine-grained structureless sandstone beds, and rare planar lamination (f4) and cross-stratification (f5). The contact surface between the alternating facies is sharp or gradational. Conglomerate beds become increasingly amalgamated upwards and grade into better sorted, through- and tangential cross-stratified pebbly sandstone (f6, Fig. 5B, Table 1). *Ophiomorpha* trace fossils (BI 0–2) occur predominantly in the upper part of the structureless sandstone beds (Fig.7B). FA2.b consists of 40–60-cm-thick cross-stratified (f5) and parallel-laminated (f4) sandstone, with common soft-sediment deformation and an absence of mud. In places, dispersed granules occur in cross-stratified sandstone beds.

FA2 units are 8–10 m thick, reveal arrangement in ~8° dipping accretionary strata in places, and grade laterally into FA3 (mouth bar – off-axis). FA2 is locally eroded and overlain by FA6 (distributary channel deposits).

Interpretation – FA2 deposits are associated with high-energy deposition close to the river mouth (e.g. Wright, 1977; Enge et al., 2010; Fidolini and Ghinassi, 2016). We interpret FA2.a as hyperpycnites (*sensu* Mulder et al., 2003) because of their position in the sedimentary system, grain size, and trends in sedimentary structures. The latter show an alternation of different conforming facies that reflect repetitive deposition from different flow types and represent deposition dominated by gravity-flow deposits (e.g. Talling et al., 2012). Deposition from debris flows transitional to high-density, stratified turbulent flows is inferred from the clast supported conglomerate with faintly visible cross-stratification (f2) (e.g. Lowe, 1982; Zavala et al., 2011; Talling et al., 2012). F2 alternates with high-density and low-density turbidity currents, as we infer from the structureless (f3) and or planar laminated or cross-stratified sandstone (f4, f5), respectively. The upward-increasing amalgamation of conglomerate beds represents an increase in energy and is interpreted as mouth bar progradation. Eventually, a decreased depth over the mouth bar causes flow deceleration (Edmonds and Slingerland, 2007), which explains the vertical transition from conglomerate beds into pebbly sandstone that reflect lower energy. Lack of finer-grained facies indicates an absence of interflood beds. The sparse occurrence of *Ophiomorpha* trace fossils supports the interpretation of a marine setting with proximity to the river outlet.

FA2.b lacks any marine indicators. However, the interpretation of mouth-bar deposition close the river outlet is supported by the gradual lateral facies change into FA3, local arrangement in dipping accretionary strata, and the lack of erosional channel-shaped surfaces.

FA2.a is dominated by gravitational-flow processes, whereas FA2.b by bedload deposition. Despite their different dominant depositional processes, they both represent a closer position relative to the feeding channel than the deposits assigned to FA3–5. This is based on the complete lack of interflood deposits (FA2.a and FA2.b) and low (FA2.a) to absent (FA2.b) bioturbation.

FA3 – Mouth bar off-axis

Description – FA3 (Fig. 8B) consists of very fine- to fine-grained, 20–50 cm thick sandstone beds that are structureless (f3, Table 1) (Fig. 5C) or show parallel lamination and tabular cross stratification (f4, f5, respectively). Soft-sediment deformation, wood fragments and stringers of extrabasinal clasts (up to 4 cm in diameter) are common. The lower part of FA3 displays rare interbedded siltstone to very fine-grained sandstone (f7). Pebbly cross-stratified sandstone (f6, Fig. 5B) dominates the upper part. Sparse

and low-diversity bioturbation (BI 0–2, *Ophiomorpha*) characterizes FA3 although rare horizontal bedding planes with BI 4–5 are present. A 20–50 cm thoroughly bioturbated sandstone bed (f9) is commonly found at the base of FA3.

FA3 units are 7–8 m thick of which the upper part locally shows arrangement in low-angle dipping accretionary strata (~3° dip towards SSW). FA3 grades laterally into FA2 (mouth bar – axis) or FA4 (mouth bar -fringe) and is locally eroded and overlain by FA6 (distributary channel deposits).

Interpretation – The sedimentary features of FA3 also indicate high energy deposition in a proximal mouth bar setting (e.g. Wright, 1977; Enge et al., 2010; Fidolini and Ghinassi, 2016). This is based on the coarsening-upward nature, the abundance of well-stratified sandstone, the accretionary architecture, and abundant soft sediment deformation. The latter indicates rapid deposition and dewatering by loading, typical for delta front deposition (e.g. Bann et al., 2008). The predominantly absent to sparse bioturbation supports the interpretation of high sedimentation rates and proximity to a river outlet (MacEachern and Bann, 2008). The *Ophiomorpha* structures are typical for high energy settings as well (Pemberton et al., 2001). The rare occurrence of thoroughly bioturbated horizontal bedding reflects short time-windows with reduced depositional energy (MacEachern and Bann, 2008), consistent with an off-axis environment. This indicates sparse interruptions of the otherwise high energy depositional setting and interpreted as the record of interflood periods.

FA4 – Mouth bar fringe

Description – A sharp tabular (at outcrop scale) nature characterizes the thin to thick (5–40 cm), very fine- to fine-grained sandstone beds of FA3 (Fig. 5D). They are structureless (f2, Table 1), but show progressively more planar- and tangential cross-stratification (f5) towards the top (Fig. 8C), where trough and cross-stratified pebbly sandstone (f6, Fig. 5B) is locally present. Sandstone beds are in places interbedded with siltstone to very fine-grained sandstone (f3), with common asymmetrical ripples (f8) (Fig. 5E). Mud-drapes are sparse. Stringers of extrabasinal clasts (up to 5 cm diameter) occur locally (Fig. 5F). The bioturbation index varies (BI 0–5) and is characterized by a non-uniform but upwards-decreasing trend. We documented high-index bioturbation predominantly on horizontal bedding planes (Fig. 7D) and/or in parallel-laminated siltstones (f7). Trace fossils observed are *Ophiomorpha, Thalassinoides, Conichnus, Palaeophycus, Macaronichnus, Teichichnus* and *Rosellia* (Fig. 7E). Thoroughly bioturbated sandstone beds (0.3–2 m thick, f9; Fig. 7F) occur locally at the base and / or at the top of FA4.

FA4 units are 6–8 m thick and grade laterally into FA3 (mouth bar – off-axis) or FA5 (mouth bar – distal fringe). Fluvial deposits (FA6) incise into FA4 locally (Fig. 9A).

Interpretation – FA4 represents episodic deposition in a position farther from the river outlet than the previous FA's. This is based on the alternation of upper and lower flow regime bedforms and the non-uniform bioturbation index. The interbedded finer-grained facies were deposited during times of lower energy between river floods (i.e., 'interflood beds' cf. Dalrymple et al., 2015; Gugliotta et al., 2016a), with preservation of a minimal tide-influence. The occurrence of intensely bioturbated horizontal bedding planes and/or interflood beds also suggests longer recurrent times with stable conditions in between deposition of individual sandstone beds (e.g. Gani et al., 2009). The upward-decreasing bioturbation index and local upward-increasing pebble content indicate bar progradation and invreasing proximity to the river mouth (e.g. MacEachern and Bann, 2008; Bhattacharya, 2010).

FA5 – Mouth bar distal fringe

Description – FA5 consists of thoroughly bioturbated sandstone beds (1–2 m thick, f9, Table 1) with or without overlying fine-grained sandstone beds with bidirectional cross-stratification (f6). The latter increase upwards in bed thickness from 10 cm to 40 cm, and bidirectionality is supported by paleocurrent measurements (n = 10) (Fig. 8D). These sandstone beds display no mud-draping or trace fossils. FA5 units have thicknesses of 3–4 m and are adjacent to FA4 (mouth bar – fringe).

Interpretation – FA5 represents mouth bar deposition with decreased river influence compared to FA2–4. The bidirectional cross-stratification indicates that tidal currents were able to fully reverse the river outflow and suggest a strong tide-influence (cf. Martinius and Gowland, 2011).

FA6 – Fluvial distributary channel

Description – FA6 consists of fine- to medium-grained sandstone bodies composed of 10–100 cm thick sandstone beds with parallel lamination, tabular (Fig. 6A) and trough cross-stratification (f5, f6, f10, Table 1). Both beds and individual foresets show normal grading and bed thicknesses decrease upwards locally. Erosional flat- and concave-upward surfaces bound the single- and multi-storey sandstone bodies, and in places they are lined with wood debris, muddy rip-up clasts, and/or pebble lag horizons (f11). The single-storey sandstone bodies have average dimensions of ~3/100 m (width/thickness). Multi-storey bodies have erosional bases that form composite surfaces bounding higher-order channel-fill elements with rare lateral accretionary packages. The multi-storey bodies are 250–300 m wide and 8–20 m thick, and consist of 2–6 stories (Fig. 9B-C). Internally, individual channel-fill elements average 4

m in preserved thickness. Varicolored mottling overprints the uppermost interval of FA6 units in places (Fig. 6B). FA6 is devoid of trace fossils, and only the top surface is commonly bioturbated with *Skolithos* (BI 0–2). Laterally continuous deposits of the Jurassic Morrison Formation also fit with this facies association, but they are outside the focus of this study. FA6 incises into mouth bar deposits (FA2-5) and is also found isolated within interdistributary-bay deposits (FA8).

Interpretation – FA6 deposition resulted from the migration of two-dimensional and three-dimensional subaqueous bedforms (dune and ripple-scale), and the formation of parallel laminations in upper flow regime conditions, within subaqueous channels (e.g. Flemming, 2000). The absence of bioturbation, marine indicators, and mud-drapes suggests deposition by fully fluvial currents. Preserved fine-grained facies within channel bodies are interpreted as abandoned channel fills, covered by interdistributary fine deposits (FA8). The varicolored mottling indicates weak pedogenesis on previously deposited channel fills and suggests prolonged subaerial exposure. Holbrook (1996) measured average channel depths of 10–12 m and widths of 90–180 m for equivalent upstream Mesa Rica trunk channels. This implies that the smaller channel dimensions of FA6 (~3/100 m width/thickness) represent the result of successive downstream bifurcations from the trunk channel. Larger channel dimensions (~250–300/~8 20 m total width/thickness) represent trunk-scale or first-order distributaries. Multi-storey channel deposits relate to repeated occupation of a given location and their deep scouring may indicate a link to forced-regression conditions.

FA7 – Tide-influenced distributary channel

Description – FA7 consists of sandstone-dominated heterolithic deposits with predominantly very fine- to fine-grained sharp-based structureless (f3, Table 1) or tabular cross-stratified sandstone beds (f5) that are 10–40 cm thick (Fig. 6C). The cross-stratification is rarely sigmoidal. These sandstone beds alternate with flaser bedding (facies 13; Fig. 6D-E) and/or thin siltstone intervals (1–10 cm thick) (f7, f8). The latter are occasionally mud-draped or double mud-draped and have unidirectional and/or bidirectional ripples in places. Wood debris, mud rip-up clasts, and syneresis cracks are common. Bioturbation occurs both in sandstone and finer-grained siltstone beds, is non-uniform and low (BI 0–3), and includes *Skolithos,* *Macaronichnus,* and *Ophiomorpha*. Erosional concave-upward surfaces bound single-storey (max. 3 m thick, 70 m wide) channel bodies. We documented one multi-storey channel body of 12/75 m (width/thickness).

FA7 occurs embedded in fine-grained interdistributary-bay deposits (FA8; Fig. 9D) and incising erosively into mouth-bar deposits (FA2–5). Paleocurrent data (n=42) reveal a mean direction towards NNW.

Interpretation – FA7 represents the infill of tide-influenced distributary channels. The heterolithic character could result from variations in fluvial discharge (Gugliotta et al., 2016a). However, the occurrence of flaser bedding can be assigned to a tidal origin (Baas et al., 2016), and all channel fills included at least two criteria that may be produced by, although not unique, to tidal processes (e.g. sigmoidal bedding, bidirectional cross-stratification, double mud-draped ripple laminae) (e.g. Nio and Yang, 1991). We therefore interpret a recurrent tide-influence of river currents, rather than a tide-dominance. The bioturbation reflects a low-diversity expression of the *Skolithos* ichnofacies, which supports the interpretation of tidally-affected deposits (Gani et al., 2009). The upstream NNW orientation of the average paleocurrent direction reflects localized tidal flood-dominance.

FA8 – Interdistributary bay

Description – FA8 consist predominantly of gray-brown muddy siltstone (f1; Fig. 6F). Very fine- to fine-grained, sharp-based sandstone beds (0.1–0.3 m thick) can be traced for 100–200 m and bed tops commonly exhibit asymmetrical ripples (f8; Fig. 7C). The sandstone beds are generally structureless (f3), ocassionally cross-stratified (f5) and interbedded with rippled siltstone (f8). Syneresis cracks common, and bioturbation (BI 0–3) includes *Skolithos, Arenicolites,* and *Phycodes*. Isolated sandstone bodies of FA6 (fluvial distributary channel) and FA7 (tide-influenced distributary channel) are found in FA8.

Interpretation – FA8 represents fine-grained lower-delta-plain to interdistributary-bay deposits, based on its close relation to FA6 and FA7, and absence of coal. The thin-bedded sheet sandstone deposits represent crevasse splays or overbank flow deposits. Trace fossils indicate short-lived marine incursions. The siltstone holds rare dinoflagellates and abundant spores and pollen (Oboh-Ikuenobe et al., 2008), which supports the interpretation of brackish conditions.

FA9 – Estuary

Description – FA9 consists of fine-grained sandstone beds (0,3–3 m) that fine upward into very fine-grained sandstone beds (5–20 cm) with interbedded siltstone in places. FA9 comprises two subsets; FA9.a is characterized by high index bioturbation (BI 5–6, *Thalassinoides, Ophiomorpha*) that obliterates primary structures and bed boundaries. Extrabasinal clasts (diameter < 3 cm) occur dispersed and locally in lag horizons (subangular-subrounded diameter 2–4 cm) together with mud rip-ups (f11, Table 1). The lags are in places overlain by a thin (~5 cm) siltstone package. FA9.b is characterized by sandstone beds (30–60 cm) that are structureless (f3) or reveal parallel lamination, tabular or trough cross-stratification (f5, f6, f9). Composite surfaces bound higher order scour surfaces and are commonly lined with wood

debris and muddy rip-up clasts. Bioturbation is absent in the lower part of FA9.a and shows an upward-increasing trend (BI 0–5) in the upper part. Trace fossils include *Thalassinoides, Ophiomorpha, Planolites* and *Teichichnus*.

FA9 has a limited lateral extent of max. 1 km and is found embedded within the underlying fluvial deposits of the Jurassic Morrison Formation; prodelta deposits (FA1) overlie FA9. FA9.a is 2–4 m thick and onlaps the the underlying strata, whereas the basal surface of FA9.b is 6–7 m thick and erosional.

Interpretation –FA9 represents estuarine deposits, based on localized occurrence, upward-increasing marine influence, and stratigraphic position below prodelta deposits (FA1) (e.g. Holbrook et al., 1987; Van Yperen et al., *in press NMGS*). The high bioturbation index of FA9.a is indicative for conditions favoring trace makers, such as wave-agitation (e.g. MacEachern and Bann, 2008). FA9.b represents the aggradational fluvial infill of existing topographic lows with a progressively increasing marine influence. The stratigraphic position of FA9 relates to the Campana Sandstone Bed (Holbrook et al., 1987).

Facies distribution

Estuarine deposits (FA3) unconformably overlie fluvial strata of the Jurassic Morrison Formation and represent the transgressive infill of topographic lows (Holbrook et al., 1987; Van Yperen et al., *in press NMGS*) (Figs 2B, 10). The overlying prodelta (FA1) deposits are present throughout the study area, except in the northwest, and separate Jurassic fluvial strata from Cenomanian Mesa Rica deposits. The latter consist of two sandstone units; Succession 1 (S1) forms a continuous sandstone sheet (6–10 m thick) throughout the study area, whereas Succession 2 (S2) is discontinuous (0–6 m thick) and embedded in interdistributary fines (FA8). S1 and S2 correlate to the lower and upper Mesa Rica, respectively Rica (e.g. Scott et al., 2004; Holbrook et al., 2006) and both successions are capped by a flooding surface with BI 1–5 (*Skolithos, Diplocraterion, Thalassinoides)* in the study area. These flooding surfaces (Maximum Regressive Surface 1 and 2) represent key stratigraphic surfaces and are used for correlation (Van Yperen et al., *in press NMGS*). They correlate to TS3.1 and TS3.2 (cf. Holbrook et al., 2006; Oboh-Ikuenobe et al., 2008).

The sheet-forming S1 contains laterally-extensive mouth bar deposits (FA2–FA5), except in the NW corner of the study area, where fluvial strata (FA6) persist. Previously published work asserted an absence of equivalent shallow marine strata up paleodepositional dip of the study area (e.g. Holbrook et al., 1987; Holbrook and Wright Dunbar, 1992) and drone data collected outside the main study area (Fig. 4) and ground truthing confirms this. The S1 is locally incised by composite erosional surfaces containing multi-storey fluvial (FA6) (Fig. 9B, C) and marine-influenced (FA7) channel infill (8–20 thick, 75–300 m

wide), and large-scale scours filled with fine-grained material (Fig. 9A). S1 thickens towards the south. The S1 / lower mesa Rica (6–10 m thick) is thin compared to both the upstream fluvial strata (10–15 m, e.g. Holbrook et al., 2006) and downstream fully deltaic strata (12–20 m, Van Yperen et al., *in press JSR*), which reflects deposition at the basin margin (Van Yperen et al., *in press NMGS*).

S2 consists of isolated composite fluvial bodies that are amalgamated into multi-lateral single or double stories. They represent mostly fully fluvial channel bodies (FA6), but tide-influenced heterolithic channel bodies occur locally (FA7) (Fig. 9D). The isolated nature of FA6 and FA7 suggests a higher A/S ratio (i.e., more accommodation or less sediment supply) than during S1 deposition. The S1 and S2 relate to the lower and upper Mesa Rica, respectively (e.g. Holbrook and Wright Dunbar, 1992; Van Yperen et al., *in press NMGS).* The overlying strata belong to the paralic Pajarito Formation (e.g. Lucas and Kisucky, 1988; Holbrook and Wright Dunbar, 1992; Holbrook, 1996; Van Yperen et al., *in press NMGS*) and are outside the scope of this paper.

Mouth bar (FA2–FA5) paleocurrents reveal a scattered pattern covering 360° variance, which we explain by the intrinsic compensation and growth in radial patterns during mouth bar development. Distributary channel deposits (FA6) show a consistent SSE component whereas the tide-influenced distributary channel deposits have a strong NNW component, supporting the interpretation of bidirectionality (Fig. 10).

MOUTH BAR ARCHITECTURE

Components

The mouth bar facies associations (FA2-5) represent deposition of sheet-like deposits in a relatively unconfined environment, based on their general lack of deep scours, the laterally extensive individual sandstone beds and the apparent tabular bed geometry. They (FA2-5) form a continuum of deposits that are interpreted as different expressions of deposition close to a river outlet. These sub-environments are referred to as ‘axis’ (FA2), ‘off-axis’ (FA3), ‘fringe’ (FA4) and ‘distal fringe’ (FA5) (Fig. 8), and represent along-strike changes of processes and resulting deposits within a single mouth bar (Fig. 11). This subdivision into mouth bar components is similar to the common classification used to describe deep-water lobe deposits that build basin-floor fan successions (e.g. Hodgson 2009; Prélat et al., 2009; Spychala et al., 2015; Hofstra et al., 2016).

Mouth bar facies associations (FA2-5) reveal a predictable trend in flow regime, bed thickness, occurrence of interflood beds, bioturbation index and tide-influence, when moving away from the center to the outer parts of the sedimentary body (Fig. 11). From mouth bar axis to fringe, the

occurrence of upper flow regime bedforms and average bed thickness diminishes. Soft-sediment deformation is most common in axis and off-axis deposits (FA2, FA3). The record of interflood beds and bioturbation index progressively increases towards the fringe (FA4; Fig. 11). Interflood beds display varying thicknesses (Fig. 12) and are expressed only by a bioturbated surface in places (Fig. 12A). These thoroughly bioturbated surfaces separate upper flow regime beds and reflect time-windows with reduced depositional energy (MacEachern and Bann, 2008). Therefore, we interpret them as formed during interflood periods, although they likely represent less time than the thicker expressions of interflood beds. In addition, some fringe sections (FA4, FA5) show thoroughly bioturbated top surfaces, which may indicate early abandonment of certain mouth bar components (Fig. 12E, F). The lack of trace fossils in axial deposits can be ascribed to the proximal deltaic setting, in which fresh water dominance overprints the marine influence and makes it unfavorable for infaunal colonization (e.g. MacEachern and Bann, 2008). If no other features indicate a shallow-marine environment, the lateral relationships described are key for an accurate identification of a mouth bar setting.

Internal geometries and stacking patterns

Geometries resulting from the progradation and aggradation of mouth bars during deposition typically reveal a predictable architectural hierarchy with basinward dipping strata at bed scale and lapping relationships at bed and element scale (e.g. Bhattacharya, 2006; Enge et al., 2010; Kurcinka et al., 2018). At bed scale, in the Mesa Rica, subtle lensoid geometries with accompanying onlapping surfaces are sparse in strike-oriented outcrops, which are characterized by a tabular nature and laterally extensive individual sandstone beds. Top truncated terminations of bedding surfaces indicate erosion due to successive bar deposition (Fig. 13). Low-angle accretionary surfaces occur in oblique-oriented sections of axis and off-axis mouth bar deposits (FA2, FA3) (Fig. 14). These oblique- to strike-oriented accretionary surfaces result from mouth bar compensational stacking and growth in radial pattern. Irrespective of their direction, accretionary surfaces are also expected in fringe and distal fringe deposits (FA4, FA5), although axial areas (FA2, FA3) are likely to develop steeper, and more evident foresets (cf. Fidolini and Ghinassi, 2016). The absence of documented accretionary surfaces in fringe sections is ascribed to the low-accommodation setting, which enforces the development of laterally widespread and very low-dipping accretionary surfaces that are difficult to resolve from outcrop data (e.g. Anell et al., 2016; Van Yperen et al., *in press JSR*).

At mouth bar scale, bars lap onto older mouth bar strata, creating inter-mouth bar bounding surfaces (Fig. 15). These bounding surfaces are subtle in places and expressed by a sharp contact between two

sand beds (Fig. 9, Log 19), or consists of a fine-grained interval mantling the older mouth bar (Fig. 14, Log 3). The latter results from prolonged lowered depositional rates before abandonment. The absence of these fine-grained packages indicates short periods between deposition of successive mouth bars. Additionally, abrupt vertical changes from typical fringe (FA4) to axial (FA2) mouth bar deposits occur in a few places and suggest a spatial shift of active bar deposition as a result of (compensational) stacking of mouth bars. Bar deposits are thicker above thinner units of the underlying mouth bar deposits (e.g. Fig. 12). This is indicative of compensational stacking, and maintenance of a topographic low while the successive mouth was being deposited (cf. Prélat et al., 2009).

DISCUSSION

Mouth bar dimensions

The distance between different mouth bar components observed in the field and their extrapolation provides an estimate of mouth bar dimensions (Fig. 16). In combination with the observed internal geometries and stacking patterns, we utilize this to assess the hierarchy of preserved geometries (Fig. 2); what are the largest elements within the S1 sheet-forming sandstone, mouth bar complexes or delta lobes?

The estimation of mouth bar dimensions is challenged by the fragmented outcrop nature and the distribution of data points (Fig. 4; Fig. 16). Log correlation reveals spatial relationships between different mouth bar components, but no complete pinch-out was documented, which limits the assessment of complete mouth bar width. Thus, an overall similar distance between mouth bar components is assumed, which gives a minimum mouth bar width. We exclude the presumable process change towards the distal fringe where sedimentation from suspension fallout would tend to create more laterally extensive plumes.

We observe a facies change from fringe to off-axis deposits and back to fringe in ~1.4 km at logs 15, 16, 17 (Fowl Canyon; Fig. 9, 16). Axial mouth bar deposits are documented at log 11 (Alamosa) and off-axis and fringe deposits at logs 12, 13 (Dog Canyon; Fig. 16). All these deposits could belong to the same mouth bar, but this causes difficulties to fit the axial mouth bar deposits at log 22 and the fringe deposits inferred from drone data ~900 m south of log 22 (Nana's; Fig. 16). We therefore separate this group of deposits in two mouth bars, of which the one in Dog Canyon has an axis-to-fringe distance of ~900 m, and thus a fringe-axis-fringe minimum width of ~1.8 km. The mouth bar at Alamosa estimates ~1.7 km.

The facies architecture and lapping relationships are consistent with components at mouth bar scale rather than depositional trends at lobe scale. We base this on the internal hierarchy, as we rarely observe bounding surfaces and lapping relationships, whilst observations at lobe scale would be expected to reveal numerous bounding surfaces because these result from the amalgamation of mouth bars. In addition, average dimensions of ancient mouth bars range from 1.1 km to 14 km wide with lengths between 2.6 km to 9.6 km (Reynolds, 1999): the inferred dimensions of individual sandstone / mouth bars in the study area (Fig. 16) fit well within this. The S1 sheet-forming mouth bar deposits thus represent amalgamation of mouth bars into a mouth bar complex (Fig. 2).

Dominant process regime of the lower Mesa Rica

Mouth bar deposits of the Mesa Rica in the study area represent river-dominated proximal deltaic deposition in a low-accommodation setting. The river-dominance is inferred from the alternation of upper and lower flow regime bedforms, the absent, low-diversity or non-uniform varying bioturbation index, and near-absence of wave-induced bedforms. Based on the latter, the wave-energy was minimal and/or dampened by river discharge.

Tidal evidence is absent in mouth bar axis and off-axis deposits (FA2, FA3). Full current-reversals represent unambiguous tidal indicators and are documented as bidirectional cross-stratification at Anna's point and occur in mouth bar distal fringe deposits (FA5) (Fig. 4, Fig. 8D). In most mouth bar fringe deposits (FA4) however, finer-grained interflood beds show mud drapes and rare upstream-migrating current ripples in places. This is inferred as evidence for (moderate) tidal modulation, although the first are not unique tidal indicators. Additionally, tidal action often extends farther landward than marine, salt-water intrusions (Dalrymple et al., 2015). The interflood beds are thoroughly bioturbated and include fully-marine trace fossils. These reflect interflood periods, in which decreased discharge allows the salinity gradient to re-establish in the off axis areas between active mouth bars (e.g. Dalrymple et al., 2015), which in turn influences the ichnological character of the deposit, resulting in more diverse trace-fossil assemblages (Gingras et al., 2002) and/or higher bioturbation indices (e.g. Gugliotta et al., 2016b; Kurcinka et al., 2018). This evidence for salt-water intrusions holds the potential tide influence.

Tide energy was variable throughout the study area, based on the differential nature and preservation of tidal indicators. Mouth bar fringes (FA4, FA5) experienced different tidal impact dependent on when and where they formed. For instance, places with weak tidal energy resulted in tidal indicators only present in fine-grained interflood beds, whereas tide-dominated areas favored formation and

preservation of sand-prone bidirectional cross-stratified sandstone beds. Both are documented in this study and suggest strike-variability in tidal energy. We reason that decreased river influence allowed localized higher tidal energy. This indicates that the 'background' tidal energy was moderate, but still only recorded in the distal mouth bar fringes, and when river discharge was low.

From mouth bar to delta front – controlling factors

The ratio between available accommodation and sediment supply (A/S) is controlled by a combination of allogenic and autogenic factors, but their contribution is often difficult to distinguish because of their close interaction, particularly at high-resolution (e.g. mouth-bar and complex) scales.

In this study, at mouth bar scale, deposition occurred within the available accommodation between previously deposited mouth bars (Fig. 15, 16). We link this to autogenic compensation processes and avulsion and/or bifurcation of distributary channels. At the same scale, we infer an overall high sediment supply from the absence of mud and silt in mouth bar axial deposits (FA2), and the rare occurrence of these in mouth bar fringe deposits (FA4, FA5; Fig. 11). Additionally, the absence of trace fossils or low-diversity assemblages (*Ophiomorpha)* in mouth bar axis to off-axis deposits (FA2, FA3) also suggests a rather continuous sedimentation rate, which prohibits colonization by trace makers. *Ophiomorpha* has been related to opportunistic colonization (e.g. Knaust and Bromley, 2012) and has been found in brackish environments and proximal deltaic settings (e.g. MacEachern and Bann, 2008). However, the alternation between upper flow regime bedforms and bioturbated surfaces or interflood beds in fringe deposits (FA4, FA5) result from variations in sediment supply. Variations in sediment supply can be caused by both autogenic and allogenic control and these are often difficult to differentiate. We link the variations to seasonal fluctuations in river discharge and to along-strike differences in sediment distribution within a mouth bar.

Amalgamated mouth bar deposits form mouth bar complexes which embody the S1 sheet forming sandstone succession. At this scale, the thinner thickness compared to both the upstream fluvial (e.g. (Holbrook, 2001; Holbrook et al., 2006), and downstream fully deltaic time-equivalent strata (Van Yperen et al., *in press JSR*), reflects deposition close to base level, with vertical limitations on aggradation and incision close to the equilibrium point of the graded stream profile (e.g. Mackin, 1948; Quirk, 1996; Holbrook et al., 2006). This is consistent with the position of the study area at the rim of the Tucumcari Basin, but also with a relatively stable, low-accommodation setting, with either constant sea-level or subjected to slow fluctuations. Limited accommodation promotes faster occupation of all available space in front of the river mouth, and thus accelerates mouth bar depositional cycles (e.g.

Olariu and Bhattacharya 2006). The low accommodation also makes lateral sedimentary accretion a prime mechanism for sediment distribution. The lateral shifting locus of mouth bar deposition means that more elapsed time is represented by preserved sediment in three dimensions than in only vertical accumulation (Miall, 2015). Each mouth bar represents a relatively short period of time but the lateral set (mouth bar complex or delta lobe) captures depositional conditions at longer time scales. Successive mouth bar coalescing in such space-limited conditions caused the sheet-like nature (cf. Olariu and Bhattacharya 2006; Van Yperen et al., *in press JSR*).

In summary, the stable base level, low-accommodation setting and position of the system in the graded stream profile, are considered the major allogenic controls on the mouth bar complex development. The limited available accommodation led to recurrent avulsion/bifurcation of distributary channels, forcing repetitive and coalescent mouth bar deposition cycles. The resultant compensational stacking and sand-dominated nature of mouth bars reflect the multi-scale interplay of allogenic and autogenic controlling factors.

Influence of low accommodation on preservation of interflood beds

Subordinate coastal processes are predominantly recorded in interflood beds. It is important to bear this in mind when interpreting competing coastal processes. If a depositional system or zone only experiences weak tidal energy, the tides modulate, rather than reverse river currents (Martinius and Gowland, 2011; Gugliotta et al., 2016b). In these settings, tidal indicators have highest preservation potential in the interflood beds (e.g. Gugliotta et al., 2016b; Kurcinka et al., 2018).

In the study area, the record of interflood beds is subordinate to the record of river flood beds. In general, more time and processes are missing than represented in the rock record (Miall, 2014). River floods have the potential to erode the interflood beds, despite floods only lasting several weeks in medium-sized rivers close to the coast (Dalrymple et al., 2015). If river flood processes are too powerful, interflood deposits are not preserved (cf. Gugliotta et al., 2016a) and the related time is not represented in the rock record. The amount of time contained in these interflood beds is significantly more than in the flood beds (e.g. Miall, 2015).

In addition to generalized ideas about preservation potential, the low-accommodation setting limits the preservation potential of interflood deposits in two ways and subsequently masks the true sedimentary processes that were active at time of deposition. First, the low accommodation increases reworking-processes at bed scale and lowers significantly the preservation potential in the axial and off-axis components. The recording of interflood deposits is thus restricted to the mouth bar fringe and distal

fringe components (FA4, FA5; Figs 1, 11) because these zones can experience temporary interruptions of the otherwise high energy depositional setting. Second, low accommodation lowers the preservation potential of the fringes themselves. The limited accommodation accelerates mouth bar depositional cycles (e.g. Olariu and Bhattacharya 2006) and increases the reworking potential of older deposits (Van Yperen et al., *in press JSR*). Mouth bar deposition with short recurrence intervals might prevent lithification of previously deposited mouth bar sediment. Additionally, reworking of fringe deposits is expected because their position will likely coincide with the higher energy zones (i.e., axis, off-axis) of successive mouth bars, as they migrate to stack compensationally (Fig. 17). Thus, the low-accommodation setting increases the potential for fringe-reworking which in turn lowers the preservation potential of interflood deposits, as these are predominantly recorded in the fringe and distal fringe mouth bar components. This also explains the sand-prone nature of the fringe and the small differences in overall grain size between mouth bar axis and fringe components. It seems unrealistic to preserve abundant fine-grained fringes in a low-accommodation system like this, but a trend in decreasing energy when moving away from the axis is evident.

Lastly, the subordinate record of interflood beds in the study area can be a result of the 'equable' climate of the mid-Cretaceous (Fluteau et al., 2007). Such a warm, low seasonality climate would imply semi-constant high river discharge conditions and could explain the dominance of river flood beds and our interpretation of a rather continuous sedimentation rate with only small variations. However, modeling studies show that there are significant uncertainties in the effect of the sea surface temperature gradient. The latter might cause Hadley cell atmospheric transport reduction which in turn enhances seasonal thermal contrasts (Fluteau et al., 2007; Hasegawa et al., 2012), causing increased variation in river discharge.

To summarize, care should be taken when evaluating the relative dominance of process regimes (i.e., river, tides, waves) in mixed systems. Especially low-accommodation settings are prone to preserve less time and deposits, and in particular the record of interflood periods. These interflood beds are the containers for recording processes captured in finer-grained facies. Their low preservation potential causes potential underestimation of the true influence of these processes in low-accommodation deltaic settings.

Implications for other deltaic studies

Our work demonstrates that axis, off-axis, fringe and distal fringe components (FA2–5) can be differentiated in river-dominated mouth bars, even in low-accommodation settings. A growing number

of studies document the variability within delta fronts (e.g. Gani and Bhattacharya, 2007; Ainsworth et al., 2016) but few document internal characteristics of mouth bar deposits and their lateral relationships (e.g. Enge et al., 2010; Jerrett et al., 2016; Fidolini and Ghinassi, 2016). Despite the different basinal settings of a shallow lake (Fidolini and Ghinassi 2016) and a foreland basin (Jerrett et al., 2016), both studies reveal similar trends as in the Mesa Rica. Finer-grained facies occur towards the fringe, diversion in paleocurrent directions, and depositional processes change from predominantly high density currents in the axial zone, to an alternation of low and high density deposits in the fringe zones.

The Campanian to Maastrichtian Horseshoe Canyon Formation (SW Alberta, Canada) is interpreted as a wave-dominated delta that transitions laterally into fluvial dominated (Ainsworth et al., 2016). The Horseshoe Canyon Formation shows strike-oriented changes in dominant processes at mouth bar complex scale, which allows assessment of the impact of these changes on mouth bar architectures, geometries and facies relationships (Ainsworth et al., 2016). We notice internal variability within individual mouth bars in the strike-oriented correlation panels (Fig. 11 in Ainsworth et al., 2016). The axial components consist of higher energy facies associations (foreshore or upper shoreface) whereas lower shoreface heterolithics become dominant towards the fringes. This demonstrates potential for differentiation of internal mouth bar components in wave-dominated deltas as well as in river-dominated deltas (this study).

The recognition of mouth bar components in this study, when compared to previous work, implies that the internal hierarchy of mouth bars is evident and observed regardless of dominant coastal processes and/or depositional setting. Subdivision of mouth bar, mouth bar complexes, and delta lobe deposits into different components can reduce complexity of models deriving from myriad facies subdivisions, and help predicting facies changes and sand distribution.

CONCLUSIONS

- The Mesa Rica Sandstone represents a river-dominated proximal deltaic succession, based on the recognition of dominant river flood beds, rare tidal-indicators, and a near-absence of wave-induced bedforms. In such a proximal setting, fresh water dominance overprints the marine influence. Lateral relationships are key for accurate identification of depositional sub-environments.
- Mouth bar deposits of the Mesa Rica Sandstone show four different mouth bar components; axis, off-axis, fringe to distal fringe, in which the occurrence of upper flow regime bedforms and average bed thickness decreases towards the fringe, whilst the record of interflood beds and bioturbation index progressively increases.

- Subdivision of mouth bars and mouth bar complexes into different components is applicable in other studies, regardless of depositional setting of the studied deltaic succession and/or dominant (deltaic) coastal processes. This improves comparisons between systems and helps predicting facies changes and sand distribution.
- The low-accommodation setting enforces a negative feedback on the preservation potential of interflood deposits. The recording of these becomes restricted to the fringe and distal fringe mouth bar components due to increased reworking-processes at bed scale and low preservation potential of these beds in the axial and off-axis low-accommodation. The preservation potential of the fringes themselves is in turn lowered because of accelerated mouth bar depositional cycles and consequent increase of fringe-reworking.
- Care should be taken when evaluating the relative dominance of process regimes (i.e., river, tides, waves) in low-accommodation settings. These are prone to preserve less time and deposits, and in particular interflood beds, yet those are the intervals that predominantly record subordinate coastal processes. Lowered preservation potential leads to underestimation of the true influence of these processes in low-accommodation deltaic settings.
- Onlapping mouth bar strata and compensational stacking patterns demonstrate the amalgamation of mouth bars into mouth bar complexes. This coalescence of mouth bars resulted in sheet-like geometries. Their sand-rich nature and near-absence of fine-grained interflood deposits reflects deposition in a low A/S setting. Deposition occurred at the rim of the Tucumcari Basin, which caused vertical limitations on aggradation and incision close to the equilibrium point of the graded stream profile.

ACKNOWLEDGEMENTS

The Lower Cretaceous basinal studies of the Arctic (LoCra) consortium and the Research Centre for Arctic Petroleum Exploration (ARCEx) allocated funding for field expeditions. Sincere thanks go to Stephen Hasiotis for essential feedback on ichnology determination, and Lina Hedvig Line, Cody Myers, Blake Warwick and Edwin Tieman for field-assistance. We thank Gretchen Gurtler and Axel Hungerbuehler from the Mesalands Dinosaur Museum and Natural Sciences Laboratory in Tucumcari for irreplaceable logistical help. Last but definitely not least, we thank the Trigg family for their hospitality and permitting us access to their property, with a special thanks to Sally, Kristen and Rick.

REFERENCES

Ainsworth, R.B., Vakarelov, B.K., MacEachern, J.A., Nanson, R.A., Lane, T.I., Rarity, F., Dashtgard, S.E. (2016) Process-Driven Architectural Variability In Mouth-Bar Deposits: A Case Study From A Mixed-Process Mouth-Bar Complex, Drumheller, Alberta, Canada. *Journal of Sedimentary Research*, 86, 512–541. https://doi.org/10.2110/jsr.2016.23

Anell, I., Lecomte, I., Braathen, A., Buckley, S.J. (2016) Synthetic seismic illumination of small-scale growth faults, paralic deposits and low-angle clinoforms: A case study of the Triassic successions on Edgeøya, NW Barents Shelf. *Marine and Petroleum Geology*, 77, 625–639. https://doi.org/10.1016/J.MARPETGEO.2016.07.005

Baas, J.H., Best, J.L., Peakall, J. (2016) Predicting bedforms and primary current stratification in cohesive mixtures of mud and sand. *Journal of the Geological Society*, 173, 12–45. https://doi.org/10.1144/jgs2015-024

Bann, K.L., Tye, S.C., Maceachern, J.A., Fielding, C.R., Jones, B.G. (2008) Ichnological and sedimentological signatures of mixed wave- and storm-dominated deltaic deposits: examples from the Early Permian Sydney Basin, Australia, in: Hampson, G.J., Steel, R.J., Burgess, P.M., Dalrymple, R.W. (Eds.), Recent Advances in Models of Siliciclastic Shallow-Marine Stratigraphy. SEPM Society for Sedimentary Geology, p. 293. https://doi.org/https://doi.org/10.2110/pec.08.90.0293

Bates, C.C. (1953) Rational theory of delta formation. *American Association of Petroleum Geologists Bulletin*, 37, 2119–2162

Bhattacharya, J.P. (2006) Deltas, Facies Models Revisited. https://doi.org/10.2110/pec.06.84.0237

Bhattacharya, J.P. (2010) Deltas, in: James, N.P., Dalrymple, R.W. (Eds.), Facies Models 4. Geological Association of Canada, pp. 233–264

Broadhead, R.F. (2004) Petroleum geology of the Tucumcari Basin—overview and recent exploratory activity. *New Mexico Geology*, 26, 90–94

Chumakov, N.M., Zharkov, M.A., Herman, A.B., Doludenko, M.P., Kalandadze, N.N., Lebedey, E.L., Rautian, A.S. (1995) Climatic belts of the mid-Cretaceous time. *Stratigraphy and Geological Correlation*, 3, 42–63

Dalrymple, R.W., Kurcinka, C.E., Jablonski, B.V.J., Ichaso, A.A., Mackay, D.A. (2015) Deciphering the relative importance of fluvial and tidal processes in the fluvial–marine transition, in: Ashworth, P.J., Best, J.L., Parsons, D.R. (Eds.), Development in Sedimentology, Fluvial-Tidal Sedimentology. Amsterdam, Elsevier, pp. 3–40. https://doi.org/10.1016/B978-0-444-63529-7.00002-X

DeCelles, P.G. (2004) Late Jurassic to Eocene evolution of the Cordilleran thrust belt and foreland basin system, western U.S.A. *American Journal of Science*, 304, 105–168. https://doi.org/10.2475/ajs.304.2.105

Dickinson, W.R. (2018) Tectonosedimentary Relations of Pennsylvanian to Jurassic Strata on the Colorado Plateau. Geological Society of America. https://doi.org/https://doi.org/10.1130/2018.2533, 2018

Edmonds, D.A., Slingerland, R.L. (2007) Mechanics of river mouth bar formation: Implications for the morphodynamics of delta distributary networks. *Journal of Geophysical Research: Earth Surface*, 112, 1–14. https://doi.org/10.1029/2006JF000574

Elliott, T. (1986) Deltas, in: Reading, H.G. (Ed.), Sedimentary Environments and Facies. Blackwell Scientific Publications, Oxford, U.K., pp. 113–154

Enge, H. D., Howell, J.A., Buckley, S.J. (2010) The geometry and internal architecture of stream mouth bars in the Panther Tongue and the Ferron Sandstone Members, Utah, U.S.A. *Journal of Sedimentary Research*, 80, 1018–1031. https://doi.org/10.2110/jsr.2010.088

Enge, Håvard D., Howell, J.A., Buckley, S.J. (2010) Quantifying clinothem geometry in a forced-regressive river-dominated delta, Panther Tongue Member, Utah, USA. *Sedimentology*, 57, 1750–1770. https://doi.org/10.1111/j.1365-3091.2010.01164.x

Fidolini, F., Ghinassi, M. (2016) Friction- and inertia-dominated effluents in a lacustrine, river-dominated deltaic succession

(Pliocene Upper Valdarno Basin, Italy). *Journal of Sedimentary Research*, 86, 1083–1101. https://doi.org/10.2110/jsr.2016.65

Flemming, B.W. (2000) The role of grain size, water depth and flow velocity as scaling factors controlling the size of subaqueous dunes. *Marine Sandwave Dynamic, International Workshop*, 55–60

Fluteau, F., Ramstein, G., Besse, J., Guiraud, R., Masse, J.. (2007) Impacts of palaeogeography and sea level changes on Mid-Cretaceous climate. *Palaeogeography, Palaeoclimatology, Palaeoecology*, 247, 357–381. https://doi.org/10.1016/J.PALAEO.2006.11.016

Gani, M.R., Bhattacharya, J.P. (2007) Basic Building Blocks and Process Variability of a Cretaceous Delta: Internal Facies Architecture Reveals a More Dynamic Interaction of River, Wave, and Tidal Processes Than Is Indicated by External Shape. *Journal of Sedimentary Research*, 77, 284–302. https://doi.org/10.2110/jsr.2007.023

Gani, R.M., Bhattacharya, J.P., MacEachern, J.A. (2009) Using ichnology to determine the relative influence of waves, storms, tides, and rivers in deltaic deposits: examples from Cretaceous Western Interior Seaway, USA, in: MacEachern, J.A., Bann, K.L., Gingras, M.K., Pemberton, S.G. (Eds.), Applied Ichnology: SEPM, Short Course Notes 52. pp. 200–255

Gingras, M.K., Räsänen, M., Ranzi, A. (2002) The significance of bioturbated inclined heterolithic stratification in the southern part of the Miocene Solimoes Formation, Rio Acre, Amazonia Brazil. *Palaios*, 17, 591–601

Gugliotta, M., Kurcinka, C.E., Dalrymple, R.W., Flint, S.S., Hodgson, D.M. (2016a) Decoupling seasonal fluctuations in fluvial discharge from the tidal signature in ancient deltaic deposits: an example from the Neuquén Basin, Argentina. *Journal of the Geological Society*, 173, 94–107. https://doi.org/doi:10.1144/jgs2015-030

Gugliotta, Marcello, Flint, S.S., Hodgson, D.M., Veiga, G.D. (2016b) Recognition criteria, characteristics and implications of the fluvial to marine transition zone in ancient deltaic deposits (Lajas Formation, Argentina). *Sedimentology*, 63, 1971–2001. https://doi.org/10.1111/sed.12291

Hasegawa, H., Tada, R., Jiang, X., Suganuma, Y., Imsamut, S., Charusiri, P., Ichinnorov, N., Khand, Y. (2012) Drastic shrinking of the Hadley circulation during the mid-Cretaceous Supergreenhouse. *Climate of the Past*, 8, 1323–1337. https://doi.org/10.5194/cp-8-1323-2012

Hodgson, D.M. (2009) Distribution and origin of hybrid beds in sand-rich submarine fans of the Tanqua depocentre, Karoo Basin, South Africa. *Marine and Petroleum Geology*, 26, 1940–1956. https://doi.org/10.1016/J.MARPETGEO.2009.02.011

Hofstra, M., Pontén, A.S.M., Peakall, J., Flint, S.S., Nair, K.N., Hodgson, D.M. (2016) The impact of fine-scale reservoir geometries on streamline flow patterns in submarine lobe deposits using outcrop analogues from the Karoo Basin. *Petroleum Geoscience*, 23, 159–176. https://doi.org/10.1144/petgeo2016-087

Holbrook, J.M. (1996) Complex fluvial response to low gradients at maximum regression; a genetic link between smooth sequence-boundary morphology and architecture of overlying sheet sandstone. *Journal of Sedimentary Research*, 66, 713–722. https://doi.org/10.1306/D42683EC-2B26-11D7-8648000102C1865D

Holbrook, J.M. (2001) Origin, genetic interrelationships, and stratigraphy over the continuum of fluvial channel-form bounding surfaces: An illustration from middle Cretaceous strata, Southeastern Colorado. *Sedimentary Geology*, 144, 179–222. https://doi.org/10.1016/S0037-0738(01)00118-X

Holbrook, J.M., Scott, R.W., Oboh-Ikuenobe, F.E. (2006) Base-level buffers and buttresses: a model for upstream versus downstream control on fluvial geometry and architecture within sequences. *Journal of Sedimentary Research*, 76, 162–174. https://doi.org/10.2110/jsr.2005.10

Holbrook, J.M., White, D.C. (1998) Evidence for subtle uplift from lithofacies distribution and sequence architecture: Examples

from lower Cretaceous strata of northeastern New Mexico, in: Shanley, K.W., McCabe, P.J. (Eds.), Relative Role of Eustasy, Climate, and Tectonism in Continental Rocks. SEPM Special Publication, pp. 123–132

Holbrook, J.M., Wright Dunbar, R. (1992) Depositional history of Lower Cretaceous strata in northeastern New Mexico : Implications for regional tectonics and depositional sequences. *Geological Society Of America Bulletin*, 104, 802–813. https://doi.org/10.1130/0016-7606(1992)104<0802

Holbrook, J.M., Wright, R., Kietzke, K.K. (1987) Stratigraphic relationships at the Jurassic-Cretaceous boundary in east-central New Mexico, in: Lucas, S.G., Hunt, A.P. (Eds.), New Mexico Geological Society, 38th Annual Fall Field Conference Guidebook. pp. 161–165

Jerrett, R.M., Bennie, L.I., Flint, S.S., Greb, S.F. (2016) Extrinsic and intrinsic controls on mouth bar and mouth bar complex architecture: Examples from the Pennsylvanian (Upper Carboniferous) of the central Appalachian Basin, Kentucky, USA. *Bulletin of the Geological Society of America*, 128, 1696–1716. https://doi.org/10.1130/B31429.1

Kisucky, M.J. (1987) Sedimentology, stratigraphy and paleogeography of the lower Cretaceous Mesa Rica delta system, Tucumcari Basin, east-central New Mexico. Albuquerque, University of New Mexico

Knaust, D., Bromley, R.G. (2012) Trace fossils as indicators of sedimentary environments, Developmen. ed. Elsevier Science

Kues, B.S. (1997) New Bivalve Taxa from the Tucumcari Formation (Cretaceous , Albian), New Mexico , and the Biostratigraphic Significance of the Basal Tucumcari Fauna Author (s): Barry S . Kues Published by : Paleontological Society Stable URL : *Journal of Paleontology*, 71, 820–839

Kurcinka, C., Dalrymple, R.W., Gugliotta, M. (2018) Facies and architecture of river-dominated to tide-influenced mouth bars in the lower Lajas Formation (Jurassic), Argentina. *AAPG Bulletin*, 102, 885–912. https://doi.org/10.1306/0609171618917155

Lowe, D.R. (1982) Sediment gravity flows: II. Depositional models with special reference to the deposits of high-density turbidity currents. *Journal of Sedimentary Petrology*, 52, 279–297

Lucas, S.., Kisucky, M.J. (1988) Type and reference sections of the Tucumcari, Mesa Rica and Pajarito Formations of east-central New Mexico. *New Mexico Geology*, 10, 82–89

MacEachern, J.A., Bann, K.L. (2008) The Role of Ichnology in Refining Shallow Marine Facies Models, in: Hampson, G.J., Steel, R.J., Burgess, P.M., Dalrymple, R.W. (Eds.), Recent Advances in Models of Siliciclastic Shallow-Marine Stratigraphy. SEPM, pp. 73–116. https://doi.org/doi:10.2110/pec.08.90.0073

MacKenzie, D.B., Poole, D.M. (1962) Provenance of Dakota Group Sandstones of the Western Interior. Wyoming Geological Association

Mackin, J.H. (1948) Concept of the graded river. *Geological Society of America Bulletin*, 59, 463–512

Martinius, A.W., Gowland, S. (2011) Tide-influenced fluvial bedforms and tidal bore deposits (Late Jurassic Lourinhã Formation, Lusitanian Basin, Western Portugal). *Sedimentology*, 58, 285–324. https://doi.org/10.1111/j.1365-3091.2010.01185.x

Miall, A.D. (2014) The emptiness of the stratigraphic record: a preliminary evaluation of missing time in the Mesaverde Group, Book Cliffs, Utah, U.S.A. *Journal of Sedimentary Research*, 84, 457–469. https://doi.org/https://doi.org/10.2110/jsr.2014.40

Miall, A.D. (2015) Updating uniformitarianism: stratigraphy as just a set of “frozen accidents.” *Geological Society, London, Special Publications*, 404, 11–36

Mulder, T., Syvitski, J.P.M., Migeon, S., Faugères, J.C., Savoye, B. (2003) Marine hyperpycnal flows: Initiation, behaviorand related deposits. A review. *Marine and Petroleum Geology*, 20, 861–882.

https://doi.org/10.1016/j.marpetgeo.2003.01.003

Nio, S.-D., Yang, C.-S. (1991) Diagnostic attributes of clastic tidal deposits: a review, in: Smith, D., Reinson, G.G.E., Zaitlin, B.A., Rahmani, R.A. (Eds.), . CSPG Special Publications, pp. 3–27

Oboh-Ikuenobe, F.E., Holbrook, J.M., Scott, R.W., Akins, S.L., Evetts, M.J., Benson, D.G., Pratt, L.M. (2008) Anatomy of epicontinental flooding: Late Albian-Early Cenomanian of the southern U.S. Western Interior Basin, in: Pratt, B.R., Holmden, C. (Eds.), Dynamics of Epeiric Seas. Geological Association of Canada, Special Paper, pp. 201–227. https://doi.org/10.1016/0016-7037(86)90064-5

Olariu, C., Bhattacharya, J.P. (2006) Terminal distributary channels and delta front architecture of river-dominated delta systems. *Journal of Sedimentary Research*, 76, 212–233. https://doi.org/10.2110/jsr.2006.026

Pemberton, S.G., Spila, M.V., Pulham, A.J., Saunders, T., MacEachern, J.A., Robbins, D., Sinclair, I. (2001) Ichnology and sedimentology of shallow and marginal marine systems: Ben Nevis and Avalon Reservoirs, Jeanne D'Arc Basin. *Geological Association of Canada, Short Course Notes*, 15, 353

Postma, G. (1990) Depositional architecture and facies of river and fan deltas: a synthesis, in: Colella, A., Prior, D.B. (Eds.), Coarse-Grained Deltas. International Association of Sedimentologists, Special Publication, pp. 13–27

Prélat, A., Hodgson, D.M., Flint, S.S. (2009) Evolution, architecture and hierarchy of distributary deep-water deposits: a high-resolution outcrop investigation from the Permian Karoo Basin, South Africa. *Sedimentology*, 56, 2132–2154. https://doi.org/10.1111/j.1365-3091.2009.01073.x

Quirk, D.G. (1996) 'Base profile': a unifying concept in alluvial sequence stratigraphy. *Geological Society, London, Special Publications*, 104, 37–49. https://doi.org/10.1144/GSL.SP.1996.104.01.04

Reynolds, A.D. (1999) Dimensions of paralic sandstone bodies. *American Association of Petroleum Geologists Bulletin*, 83, 211–229

Scott, R.W. (1974) Bay and shoreface benthic communities in the Lower Cretaceous. *Lethaia*, 7, 315–330. https://doi.org/10.1111/j.1502-3931.1974.tb00907.x

Scott, R.W., Holbrook, J.M., Oboh-Ikuenobe, F.E., Evetts, M.J., Benson, D.G., Kues, B.S. (2004) Middle Cretaceous stratigraphy, southern western interior seaway, New Mexico and Oklahoma. *Rocky Mountain Association of Geologists*, 41, 33–61

Scott, R.W., Oboh-ikuenobe, F.E., Benson, D.G., Holbrook, J.M. (2009) Numerical age calibration of the Albian/Cenomanian boundary. *Stratigraphy*, 6, 17–32

Scott, R.W., Oboh-Ikuenobe, F.E., Benson, D.G., Holbrook, J.M., Alnahwi, A. (2018) Cenomanian-Turonian flooding cycles: U.S. Gulf Coast and Western Interior. *Cretaceous Research*, 89, 191–210. https://doi.org/10.1016/J.CRETRES.2018.03.027

Spychala, Y.T., Hodgson, D.M., Prélat, A., Kane, I.A., Flint, S.S., Mountney, N.P. (2017) Frontal and Lateral Submarine Lobe Fringes: Comparing Sedimentary Facies, Architecture and Flow Processes. *Journal of Sedimentary Research*, 87, 75–96. https://doi.org/10.2110/jsr.2017.2

Talling, P.J., Masson, D.G., Sumner, E.J., Malgestini, G. (2012) Subaqueous sediment density flows: Depositional processes and deposit types. *Sedimentology*, 59, 1937–2003. https://doi.org/10.1111/j.1365-3091.2012.01353.x

Taylor, A.M., Goldring, R. (1993) Description and analysis of bioturbation and ichnofabric. *Journal of the Geological Society*, 150, 141–148. https://doi.org/10.1144/gsjgs.150.1.0141

Waage, K.M. (1955) Dakota Group in northern Front Range foothills, Colorado. *U.S. Geological Survey Professional Paper*, 274-B, B15–B51

Wellner, R., Beaubouef, R., Van Wagoner, J., Roberts, H., Sun, T. (2005) Jet-plume depositional bodies - The primary building

blocks of the Wax Lake Delta. *Gulf Coast Association of Geological Societies,Transactions*, 55, 867–909

Wright, L.D. (1977) Sediment transport and deposition at river mouths: A synthesis. *Geological Society of America Bulletin*, 88, 857–868

Wright, L.D., Coleman, J.M. (1973) Variations in morphology of major river deltas as functions of ocean wave and river discharge regimes, American Association of Petroleum Geologists Bulletin. American Association of Petroleum Geologists. https://doi.org/10.1306/819A4274-16C5-11D7-8645000102C1865D

Zavala, C., Arcuri, M., Di Meglio, M., Diaz, H.G., Contreras, C. (2011) A genetic facies tract for the analysis of sustained hyperpycnal flow deposits, in: Slatt, R.M., Zavala, C. (Eds.), Sediment Transfer from Shelf to Deep Water—Revisiting the Delivery System. AAPG Studies in Geology, pp. 31–52. https://doi.org/10.1306/13271349St613438

Van Yperen, A.E., Holbrook, J.M., Poyatos-Moré, M., Midtkandal, I., in press, Coalesced delta front sheet-like sandstone bodies from highly avulsive distributary channels: the low-accommodation Mesa Rica Sandstone (Dakota Group, New Mexico, USA), Journal of Sedimentary Research

Van Yperen, A.E., Line, L.H., Holbrook, J.M., Poyatos-Moré, M., Midtkandal, I., in press, Revised stratigraphic relationships of the Dakota Group in the Tucumcari Basin (San Miguel county, New Mexico, USA), 70th ed. New Mexico Geological Society Guidebook

Summary of facies (f) in the studie d interval at the Trigg Ranch study area, east- central New Mexico

	Description	Grainsize	Structures	Biogenic structures	Interpretation
f1	Muddy siltstone	Mud - Si	Structureless, gray or gray-brown muddy siltstone. In places fissile. Max 5 m thick. Commonly vegetated.	BI 4–6: *Phycosiphon, Thalassionoides, Planolites, Teichichnus, Chondrites, Helminthopsis.* Locally, no bioturbation observed.	Suspension fallout, low sedimentation rates in an open marine setting (bioturbated), or brackish setting (non-bioturbated).
f2	Conglomerate	Cgl	Sharp-based, clast-supported, conglomerate, often crudely stratified. No or normal grading. Sub-angular to sub-rounded, poorly - moderately sorted extrabasinal and intrabasinal clasts, average ø 0,5–2 cm (max ø 6 cm). Extrabasinal clasts are predominantly quartz and chert. Fine- to medium-grained matrix. Bed thickness 10–30 cm.	BI 0–2: *Ophiomorpha*	Predominantly deposition from high-density turbidity currents. When grading and stratification is absent; deposition from debris flows transitional to high-density turbulent flow.
f3	Structureless sandstone	VF - F	Erosional, sharp-based, structureless sandstone with normal grading. Bed tops exhibit asymmetrical ripples locally. Bed thickness 5–80 cm.	BI 0–5: *Ophiomorpha, Skolithos, Thalassionoides, Conichnus, Palaeophycus, Rosellia* . High BI-indices on horizontal bedding planes.	Lack of structure might be due to intensive surface weatering. Rapid suspension fall out. Waning flow energy when rippled top surface.
f4	Parallel-laminated sandstone	VF - F	White and brown sharp-based and -topped, parallel-laminated sandstone. Bed tops exhibit asymmetrical ripples locally. Bed thickness 20–70 cm.	BI 0–3: *Skolithos, Ophiomorpha, Rossellia*	Upper flow conditions
f5	Tabular cross-stratified sandstone	VF - M	Sharp-based and -topped, local lower erosive base, planar and tangential tabular cross-stratified sandstone. Locally, bidirectional. Bed thickness 20–50 cm. In places organized in low-angle accretionary packages. Local wood-remains.	BI 0–4: *Ophiomorpha, Skolithos, Thalassionoides, Conichnus, Palaeophycus, Rosellia* . High BI-indices on horizontal bedding planes.	Migrating straight-crested or sinuous dunes with and without flow saperation, lower flow regime.
f6	Pebbly sandstone	F - F-M	Pebbly sandstone with trough and tangential cross-stratification. Intra- and extrabasinal pebbels, average ø 0,5–1 cm (max ø 3 cm). In places organized in low-angle accretionary packages.	*Not observed*	High-energy unidirectional traction currents and bed load deposition.
f7	Parallel-laminated siltstone	Si - VF	Parallel-laminated silstone, in places mud-draped. 1–20 cm thick.	*Not observed*	Gentle flow activity with potential tide-influence.
f8	Asymmetrical ripple-laminated siltstone to sandstone	VF - F	Unidirectional current ripples in sharp-based sandstone beds. Sparse climbing and/or sigmoidal ripples. Bed thickness 3–40 cm.	BI 0–3*: Skolithos, Ophiomorpha, Macharonichnus*	Migrating straight-crested ripples. Lower flow regime. Climbing ripples indicate high rates of deposition.
f9	Thoroughly bioturbated sandstone	Si - F	Sharp-based and -topped sandstone beds. Bioturbation obliterates original sedimentary features and bed boundaries. 20 cm–3 m thick.	BI 5–6: *Thalassionoides, Ophiomorpha*	Bioturbation favourable conditions (optimized oxygen, salinity, temperature).
f10	Trough cross-stratified sandstone	F - M	Single to several sets of trough cross-bedding. Set thickness 15–110 cm.	*Not observed*	Migrating sinuous or linguoid dunes. Lower flow regime.
f11	Pebble lag	Cgl	Erosional basal surface with extrabasinal clasts in a finer sandstone matrix. Clast- or matrix-supported, subangular to subrounded. Includes mud-silt rip-up clasts and/or wood debris locally.	*Not observed*	High-energy fluvial channel base. When situated at the base of facies structureless or muddy siltstone, potential lag formed by wave-erosion and reworking.
f12	Paleosol	Si - Vf	Purple siltstone with gray rhizoliths and yellow mottling. Yellow-grey siltstone with yellow mottling. Locally, soil development overprints parallel-laminated sandstone.	Mottling, rhizoliths	Subaerial exposure, post-deposition weak to moderate pedogenic development.
f13	Flaser bedding	VS-F	Ripple- and dune-scale cross-stratified sandstone with single or double mud drapes. Locally, climbing ripples and / or bidirectional ripples.	BI 0–1: *unidentified*	Current reversals in subtidal zone. Climbing ripples indicate high rates of deposition.

FIGURE CAPTIONS

FIGURE 1 Schematic depiction of facies stacking patterns with seasonal bedding (i.e., river flood and interflood beds). River flood beds are thicker and more amalgamated towards the top and in the proximal part of the mouth bar. A progressive decrease of preserved interbedding shows a similar trend. Note that the occurrence of interflood beds is expected to be lower in the scenario with a lower A/S ratio. Modified after Gugliotta et al. (2016a).

FIGURE 2 Coalescence of individual mouth bars forms mouth bar complexes and delta lobes, which together form the building blocks of a delta system. Mouth bar complexes are related to the same pulse of progradation and their shallow distributary channel network are genetically linked. Mouth bar lobes consist of mouth bar complexes related to the same primary distributary feeder channel. Note that the occurrence of fringe deposits is limited in proximal areas at all scales. Terminology used in previous works and cited in the text is listed.

FIGURE 3 (A) Regional map of the Western Interior during the Early – Late Cretaceous (Albian-Cenomanian) showing the approximate location of the Western Interior Seaway extent (light blue, Blakey, 2014) and main basins that formed during Laramide Orogeny and Colorado Orogeny (modified after Van Yperen et al. *in press-JSR*). The study area is situated at the rim of the Tucumcari Basin (red square). GRB = Green River Basin; UB= Uinta Basin; DB (Colorado) = Denver Basin; SJB = San Juan Basin, TB = Tucumcari Basin; DB (New Mexico) = Dalhart Basin; BD = Bravo Dome. (B) Chronostratigraphic chart for the Jurassic to Cenomanian successions in Northeastern (NE) and East-central New Mexico. References used for compilation; Waage, 1955; Holbrook et al., 2006; Oboh-Ikuenobe et al., 2008; Van Yperen et al., JSR; Van Yperen et al., NMGS. Albian-Cenomanian boundary from Scott et al. (2018). SB = Sequence boundary, TS = Transgressive Surface

FIGURE 4 Geologic map of the study area around the Trigg Ranch, in San Miguel County, showing the outcrop extent and location of the collected dataset. Drone data was collected outside the main study area as well (see inset). Locations of the photopanoramas in Fig. 13, 14 and 15 are also indicated.

FIGURE 5 Photographs of selected facies (Table 1). (A) Clast supported conglomerate (f2) alternating with structureless sandstone (f3) and/or planar lamination (f4) or cross-stratification (f5). The contact

represents an erosive surface related to the reworking of successive bypassing events. This facies assemblage occurs in axial mouth-bar deposits (FA2). (B) Trough cross-stratified pebbly sandstone (f6) in axial mouth-bar deposits (FA2). Common in off-axis deposits (FA3) as well. (C) Structureless sandstone (f3) with wood fragments and low index bioturbation (BI 1) in mouth-bar off-axis deposits (FA3). Common in mouth-bar fringe deposits (FA4) as well. O = *Ophiomorpha*. (D) Thin to thick-bedded (5–40 cm), fine-grained structureless sandstone (f3) and cross-stratified sandstone (f5) in mouth bar fringe (FA4) deposits. Interbedding with asymmetrical ripple-laminated sandstone (facies 8). (E) Structureless sandstone (f3) interbedded with asymmetrical ripple-laminated sandstone (f8), with high-index bioturbation on horizontal bedding planes. This is typical for mouth bar fringe deposits (FA4). (F) Bioturbated parallel laminated sandstone (f4) with scarttered pebble lags in mouth bar fringe deposits (FA4). O = *Ophiomorpha.* 15-cm pencil and 33-cm hammer for scale.

FIGURE 6 Photographs of selected facies (Table 1). (A) Bedsets of tabular cross-stratified sandstone (f5) in fluvial distributary channel-fill deposits (FA6). (B) Weak pedogenesis overprinting parallel-laminated sandstone (f6) at the top of a fluvial distributary channel fill (FA6). (C) Tide-influenced distributary channel-fill deposits (FA7), with bidirectional tabular cross-stratified sandstone (f5) and ripple-laminated sandstone (f8), overlying sand-dominated heterolithic deposits (f3, f13). (D) Flaser bedding (f13) with climbing ripples and upwards-increasing sand content, in tide-influenced distributary channel-fill deposits (FA7). (E) Zoom-in of c, with detail of flaser bedding (f13). (F) Gray-brown muddy siltstone (f1), interpreted as part of interdistributary bay deposits (FA8). 15-cm pencil and 33-cm hammer for scale.

FIGURE 7 Photographs of selected ichnotaxa. (A) Muddy siltstone with BI 4–5 in prodelta deposits (FA1). (B) Alternating conglomerate (f2) and structureless sandstone (f3) with non-uniform BI 0–3 in axial mouth-bar deposits (FA2). (C) Structureless sandstone beds with bed tops that exhibit asymmetrical ripples (f3) interbedded with silt to very-fine-grained sandstone (f7). Trace fossils include *Skolithos* and several undefined traces. This facies and trace fossil assemblage occur in interdistributary bay deposits (FA8). (D) High-index (BI 4–5) bioturbation at a basal bedding plane in mouth-bar fringe deposits (FA4). (E) Low-diversity trace fossil suite in mouth bar off-axis to fringe deposits (FA3, FA4). (F) Thoroughly bioturbated sandstone (BI 5–6) in which traces are only sporadically identifiable. (G) Bioturbated top surface in mouth-bar off-axis deposits (FA3). Th = *Thalassinoides*, He = *Helminthopsis*, Pl = *Planolites*, S = *Skolithos*, O = *Ophiomorpha*, Pa = *Palaeophycus*, C = *Conichnus*, R = *Rosselia*. 15-cm pencil and 33-cm hammer for scale.

FIGURE 8 Mouth bar facies associations (FA2-FA5) in the low-accommodation Mesa Rica deltaic system. Selected photographs show representative parts or complete logged sections of the different sub-environments referred to as 'axis' (FA2), 'off-axis' (FA3), 'fringe' (FA4), and 'distal fringe' (FA5). Bidirectional paleocurrent measurements support the interpretation of tide-influenced distal fringe deposits (D).

FIGURE 9 Photographs of fluvial facies associations that occur in the S1 and S2 successions. (A) Fine-grained abandoned channel fill incising S1 mouth bar deposits. Location: Rain Ridge (Fig.4). (B) Multistory fluvial distributary channel (FA6) bound by composite erosional surface, within the S1. Location: Anna's point (Fig. 4). (C) Interpretation and line drawing of b. The multistory fluvial body incises into the underlying Juarrasic Morrison Formation. (D) Heterolithic deposits interpreted as tide-influenced distributary channel fill (FA7), in S2. Location: Fowl Canyon (Fig. 4)

FIGURE 10. Correlation fence diagram illustrating 3D facies distribution offered by physical correlation and interpolation of strike-oriented cross sections. Map shows the true orientation and distances, whereas the diagram is simplified ed to maximize clarity. Today's topography is visualized, except for the S1 succession because this is the main focus of the paper. The MRS2 is used as a datum for the fence diagram. Sketch logs are not depicted and rose diagrams display paleocurrent data from S1 grouped according to facies associations. MRS = Maximum Regressive Surface.

FIGURE 11 Schematic representation of a strike-oriented cross-section through an individual mouth bar indicating the distinguished components. Displayed logs are taken from originally measured logs to enhance differences between components. Mouth bar axis to distal fringe trends reveal changes in flow regime, bed thickness, occurrence of interflood beds, bioturbation index, and tide-influence. Not all fringe components show tide-influence. An increase in tide-influence (imaged by bidirectional cross-stratification, right limb of the mouth bar) is accompanied with a decreasing bioturbation index. See text for further discussion.

FIGURE 12 River flood and interflood beds in FA4 deposits (mouth-bar fringe). River flood beds have a sharp base, coarser grain size and lower bioturbation index (BI 0–3) than interflood deposits. In places, the interflood is represented only by a thoroughly bioturbated surface (a). Bioturbated horizons

936 commonly require several months to form (e.g. Gringras et al., 2002) and contrast with upper flow
937 regime beds interpreted as river flood event beds, which can be as short as a few hours (Gugliotta et al.,
938 2016a and references herein). Note that the upper part of the facies association is thoroughly
939 bioturbated in e, f which indicates early abandonment. Th = *Thalassinoides*, R = *Rosselia.* 15-cm pencil
940 for scale.
941
942 FIGURE 13 (a) Field photograph showing along-strike internal mouth bar geometries. The white arrow
943 indicates average palaeocurrent direction. Inset box shows location of b. (b) Zoom in on subtle lensoid
944 geometries. (c) Subtle lensoid geometries show accompanying onlapping, downlapping, and truncation
945 relationships.
946
947 FIGURE 14 Field photograph (and interpretation) of a mouth bar section, showing low-angle
948 accretionary surfaces (clinoforms) top-truncated by distributary channels. Note the cross-stratification
949 that is locally in opposite direction than larger accretionary surfaces. Clinoforms could evidence oblique
950 compensational growth of mouth bars as these are complex geobodies that grow in a radial pattern. See
951 Figs 4, 10 for location. See text for further discussion.
952
953 FIGURE 15 (A) Strike-oriented photograph, see Figs 4, 10 for location. (B) Line drawing and
954 interpretation of A, showing onlapping relationships between bed sets. (C) Vertical exaggeration of B,
955 enhancing onlapping relationships (red arrow). The mouth bar laps onto older fringe strata, creating
956 inter-mouth bar bounding surfaces. This represents the bounding surface between two individual mouth
957 bars in which the younger mouth bar onlaps the off-axis and fringe sections of the previous. Note that
958 the older mouth bar shows lateral facies transitions from heterolithic fringe (D), to sand-prone off-axis
959 deposits (E), to mouth bar axis deposits with common soft sediment deformation and an absence of
960 trace fossils (F).
961
962 FIGURE 16 (A) Mouth bars range 1.4–1.8 km, based on the distribution of mouth bar components,
963 distributary channels and interpolation between them. Where no mouth bar abbreviation is indicated,
964 strata are eroded by trunk channels. These trunk channels are not visualized in the figure as these
965 reflect a later generation and feed a delta outside and down-dip of the study area. Paleocurrent
966 readings were collected from mouth bar deposits. (B) Schematic representation of the relationship

between two individual mouth bars. This is based on observed abrupt vertical changes, which we interpreted as a spatial shift and stacking of individual mouth bars.

FIGURE 17: From individual mouth bar to mouth bar complex. (A) A single mouth bar shows decreasing river jet strength and increase in recording of interflood beds from axis to distal fringe. (B) Mutiple mouth bars occupy all available accommodation. Every stage (t1-t4) shows the cumulative preservation of river jet deposits and interflood beds. Successive deposition of mouth bars causes reworking of fringes and subsequently erodes the previously deposited interflood beds, thererby the potential recording of subordinate coastal processes. (C) Eventually, a primary distributary channel erodes through the mouth bar complex and will intiate new mouth bar deposition beyond the stranded mouth bar complex.

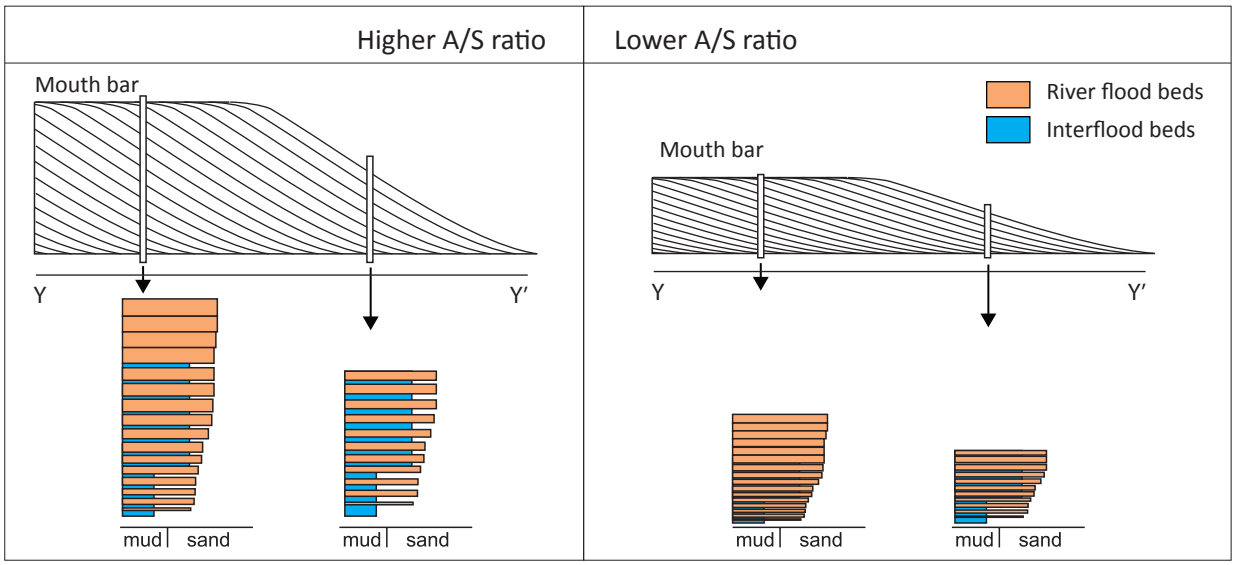
Higher A/S ratio
Lower A/S ratio
Mouth bar
River flood beds
Interflood beds
Mouth bar
Y
Y′
Y
Y′
mud
sand
mud
sand
mud
sand
mud
sand

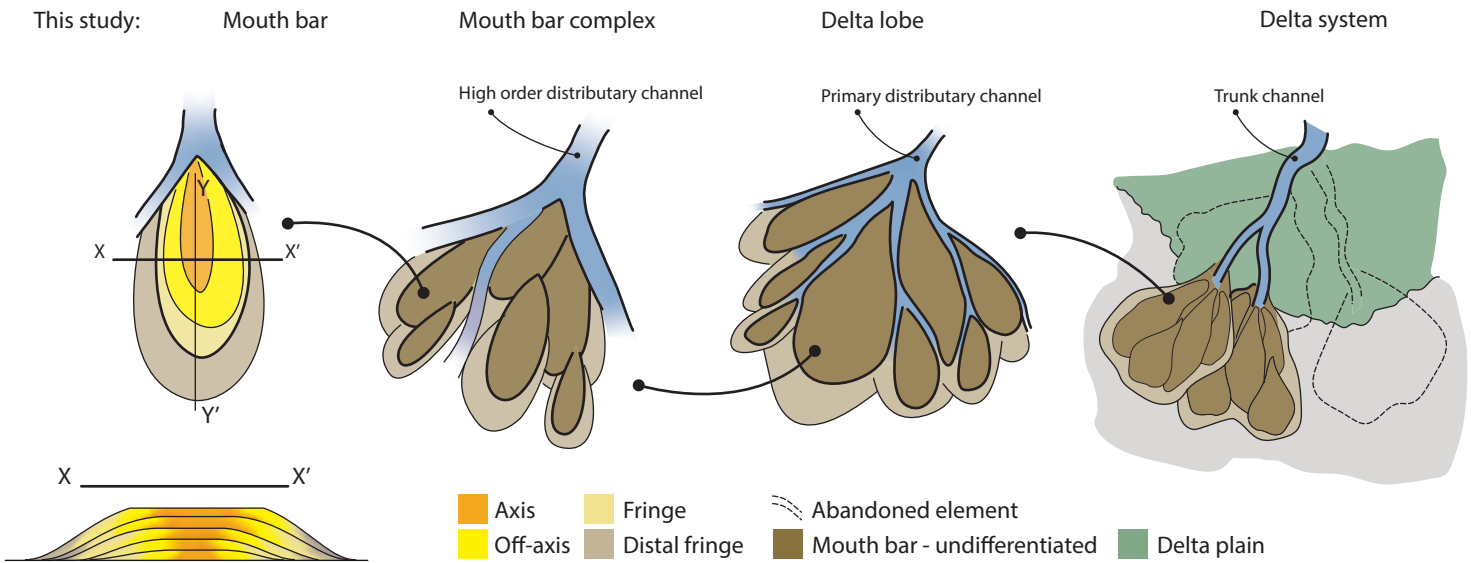

(Stream) mouth bar	Mouth bar complex / Bar assemblages	Delta lobe	Enge et al., 2010
Mouth bar	Mouth bar complex	Delta lobe	Kurcinka et al., 2018 Jerrett et al., 2018
Jet deposit	Jet deposit complex / Sub-lobe	Delta lobe	Wellner et al., 2005
Mouth bar element set	Mouth bar element complex	Element complex set	Ainsworth et al., 2016

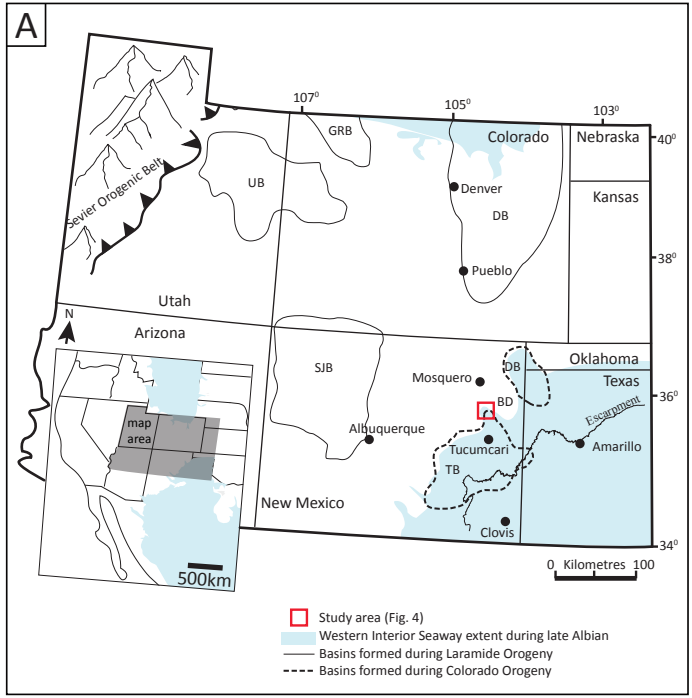
A
107°
105°
103°
40°
38°
36°
34°
GRB
UB
Sevier Orogenic Belt
Colorado
Nebraska
Kansas
Denver
DB
Pueblo
Utah
Arizona
N
map area
SJB
Mosquero
DB
BD
Albuquerque
Tucumcari
TB
Oklahoma
Texas
Escarpment
Amarillo
New Mexico
Clovis
500km
0 Kilometres 100
Study area (Fig. 4)
Western Interior Seaway extent during late Albian
Basins formed during Laramide Orogeny
Basins formed during Colorado Orogeny

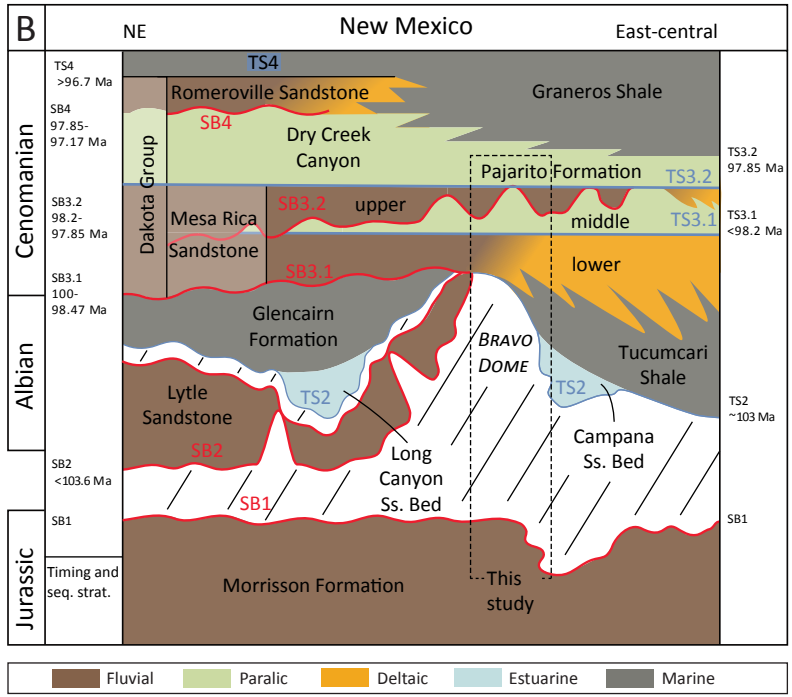
B
NE
New Mexico
East-central
Cenomanian
Albian
Jurassic
TS4
>96.7 Ma
SB4
97.85-
97.17 Ma
SB3.2
98.2-
97.85 Ma
SB3.1
100-
98.47 Ma
SB2
<103.6 Ma
SB1
Timing and seq. strat.
TS4
Romeroville Sandstone
Graneros Shale
SB4
Dry Creek
Canyon
Dakota Group
Pajarito Formation
TS3.2
97.85 Ma
SB3.2
upper
Mesa Rica
Sandstone
middle
TS3.1
<98.2 Ma
SB3.1
lower
Glencairn
Formation
BRAVO
DOME
Tucumcari
Shale
TS2
~103 Ma
Lytle
Sandstone
TS2
SB2
Long
Canyon
Ss. Bed
Campana
Ss. Bed
SB1
Morrisson Formation
This
study
Fluvial
Paralic
Deltaic
Estuarine
Marine

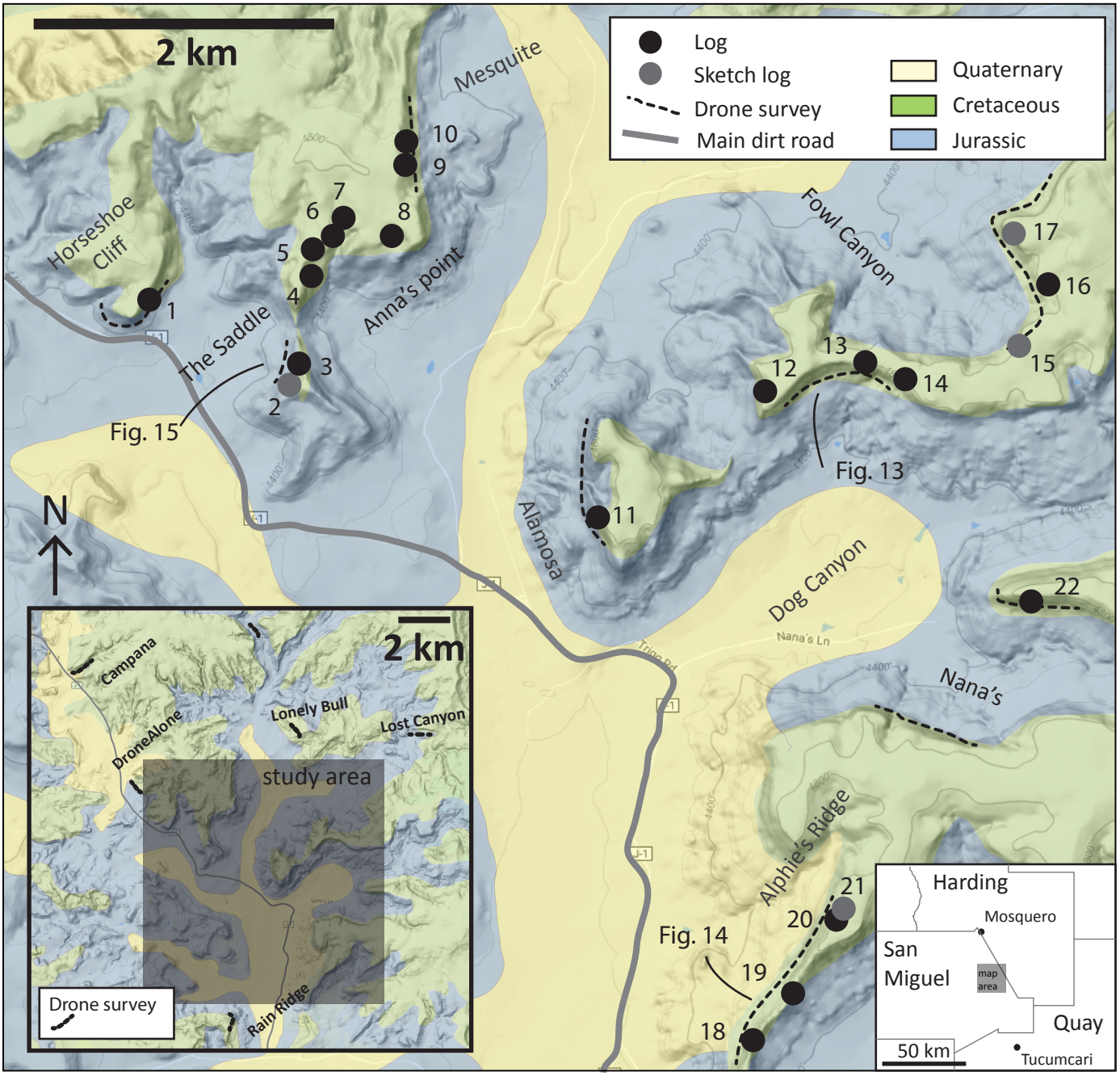
2 km
Log
Sketch log
Drone survey
Main dirt road
Quaternary
Cretaceous
Jurassic
Mesquite
Horseshoe Cliff
Anna's point
The Saddle
Fig. 15
Fowl Canyon
Fig. 13
Alamosa
Dog Canyon
Nana's Ln
Nana's
Alphie's Ridge
Fig. 14
N
1
2
3
4
5
6
7
8
9
10
11
12
13
14
15
16
17
18
19
20
21
22
2 km
Campana
DroneAlone
Lonely Bull
Lost Canyon
study area
Drone survey
Rain Ridge
Harding
Mosquero
San Miguel
map area
Quay
50 km
Tucumcari

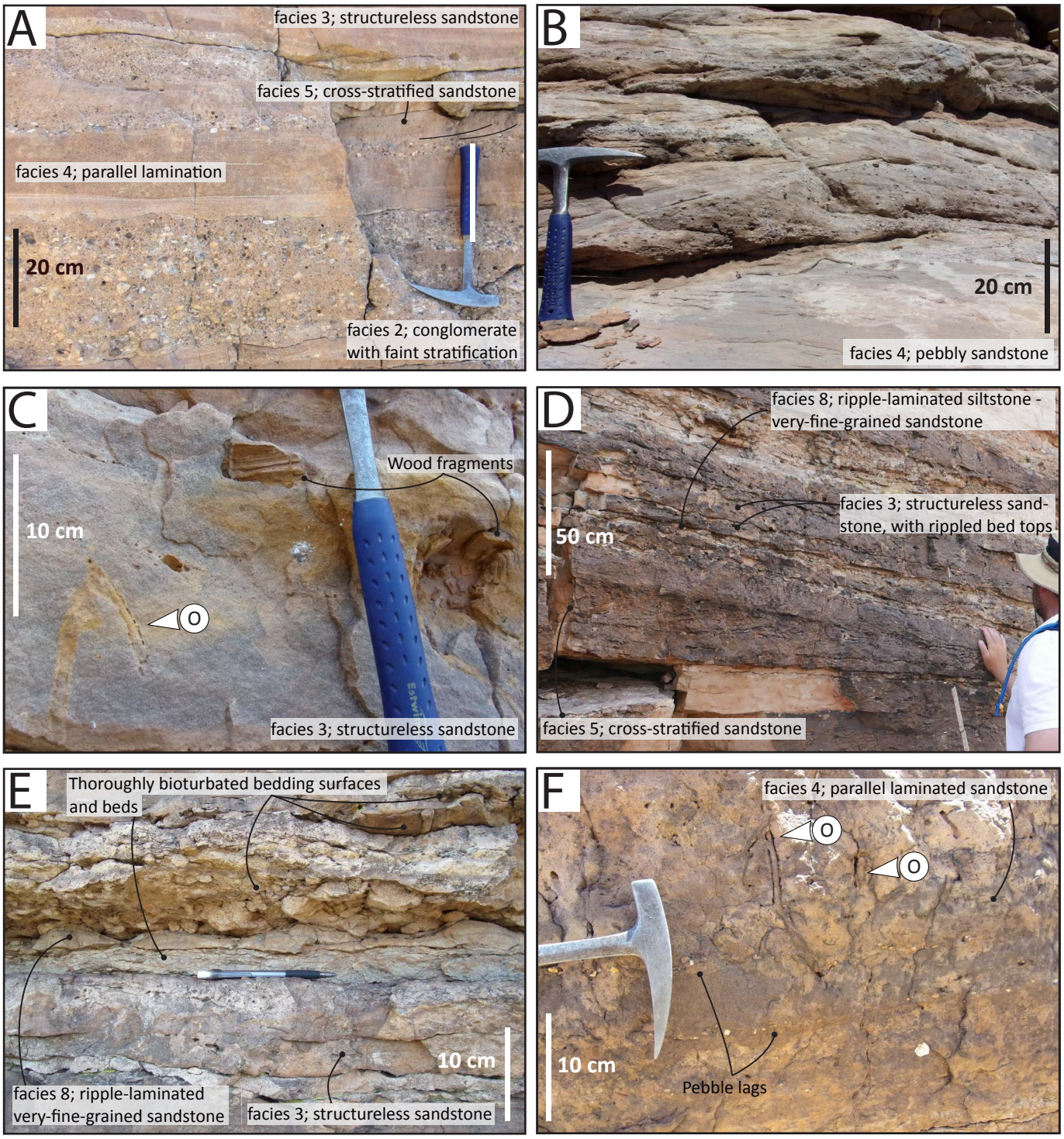
A
facies 3; structureless sandstone
facies 5; cross-stratified sandstone
facies 4; parallel lamination
20 cm
facies 2; conglomerate with faint stratification
B
20 cm
facies 4; pebbly sandstone
C
Wood fragments
10 cm
facies 3; structureless sandstone
D
facies 8; ripple-laminated siltstone - very-fine-grained sandstone
facies 3; structureless sand-stone, with rippled bed tops
50 cm
facies 5; cross-stratified sandstone
E
Thoroughly bioturbated bedding surfaces and beds
10 cm
facies 8; ripple-laminated very-fine-grained sandstone
facies 3; structureless sandstone
F
facies 4; parallel laminated sandstone
10 cm
Pebble lags

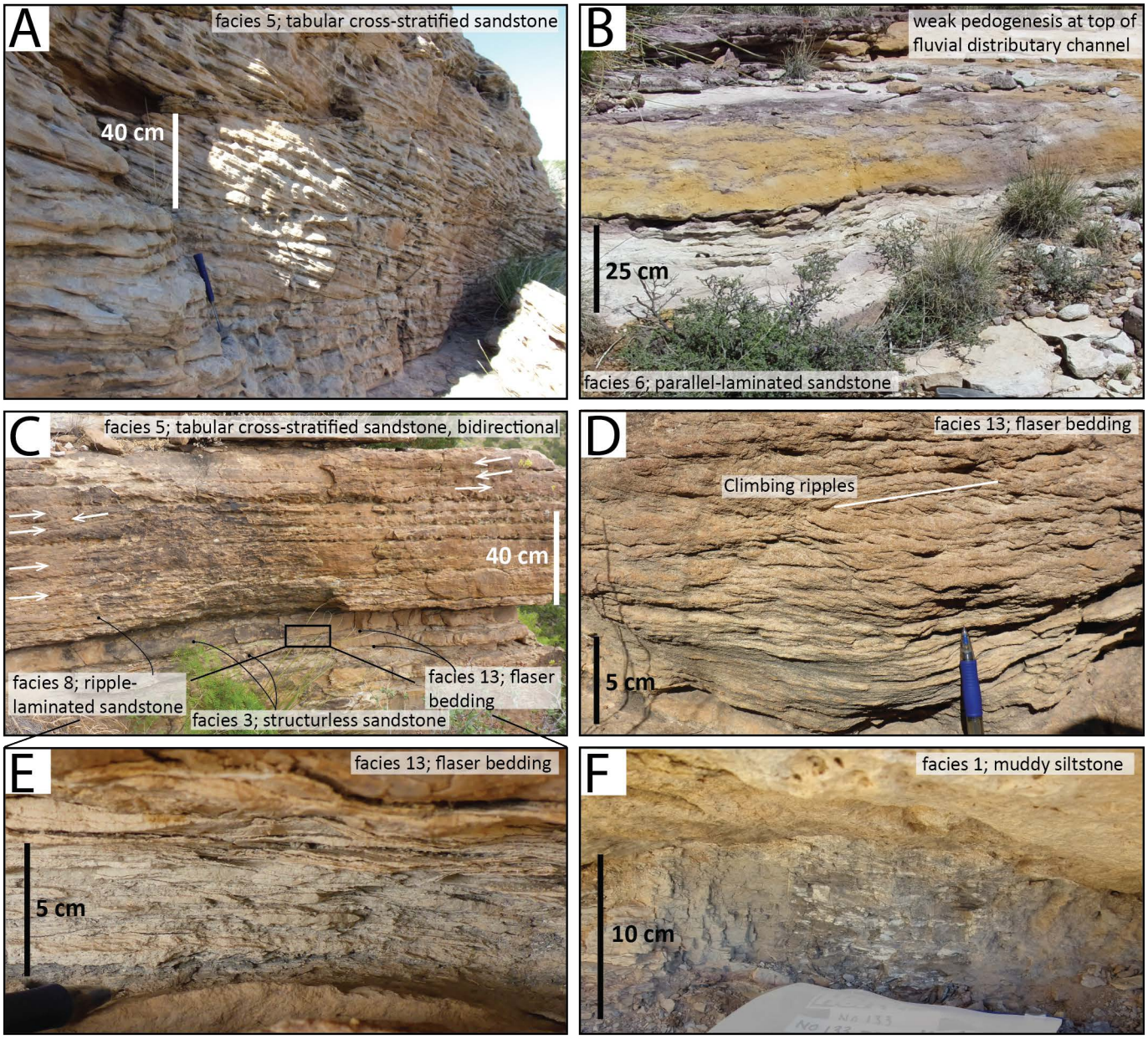
A
facies 5; tabular cross-stratified sandstone
40 cm
B
weak pedogenesis at top of fluvial distributary channel
25 cm
facies 6; parallel-laminated sandstone
C
facies 5; tabular cross-stratified sandstone, bidirectional
40 cm
facies 8; ripple-laminated sandstone
facies 3; structurless sandstone
facies 13; flaser bedding
D
facies 13; flaser bedding
Climbing ripples
5 cm
E
facies 13; flaser bedding
5 cm
F
facies 1; muddy siltstone
10 cm

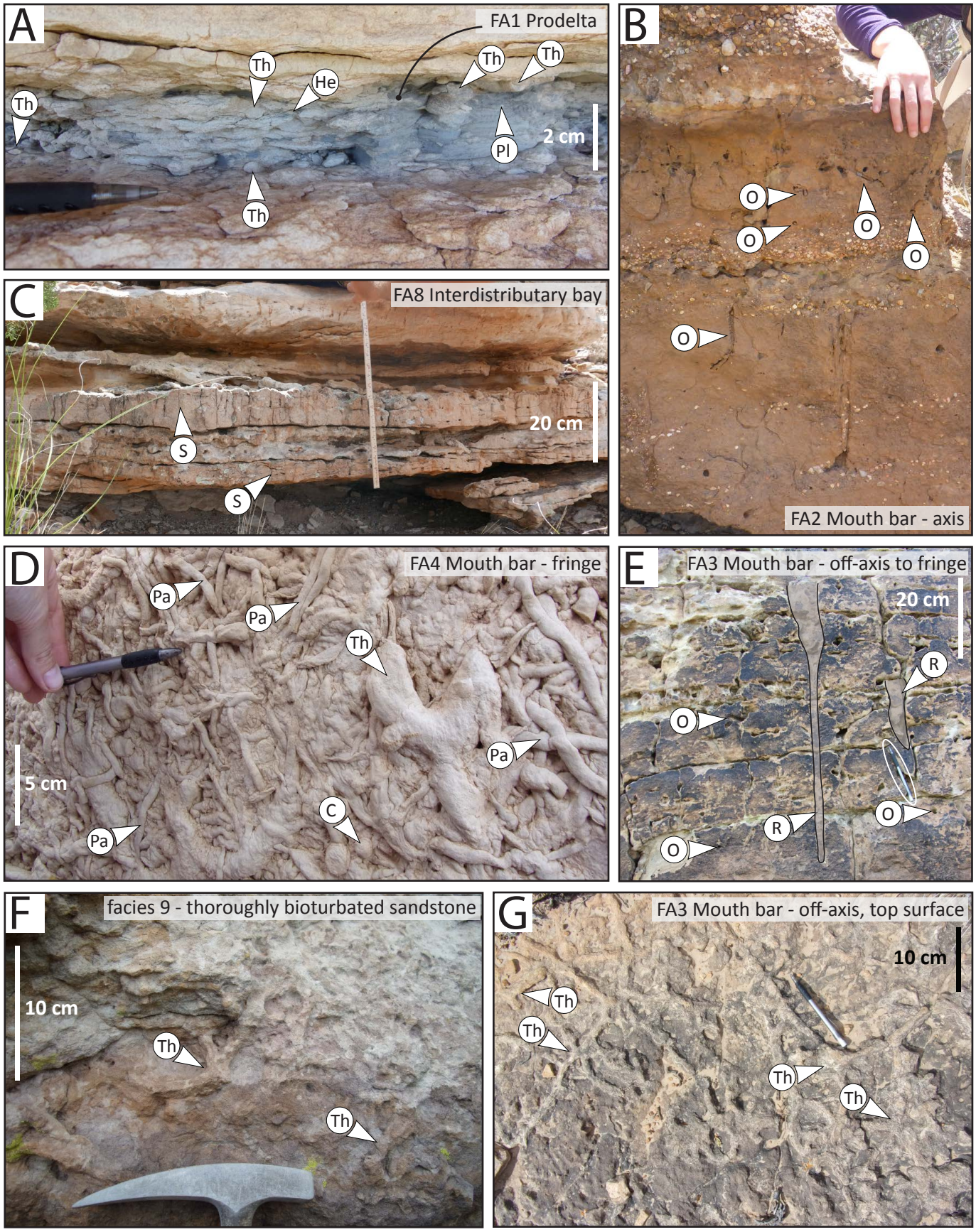
A
FA1 Prodelta
Th
He
Th
Th
Th
Pl
2 cm
Th
B
O
O
O
O
FA2 Mouth bar - axis
C
FA8 Interdistributary bay
20 cm
S
S
D
FA4 Mouth bar - fringe
Pa
Pa
Th
Pa
5 cm
C
Pa
E
FA3 Mouth bar - off-axis to fringe
20 cm
R
O
R
O
O
F
facies 9 - thoroughly bioturbated sandstone
10 cm
Th
Th
G
FA3 Mouth bar - off-axis, top surface
10 cm
Th
Th
Th
Th

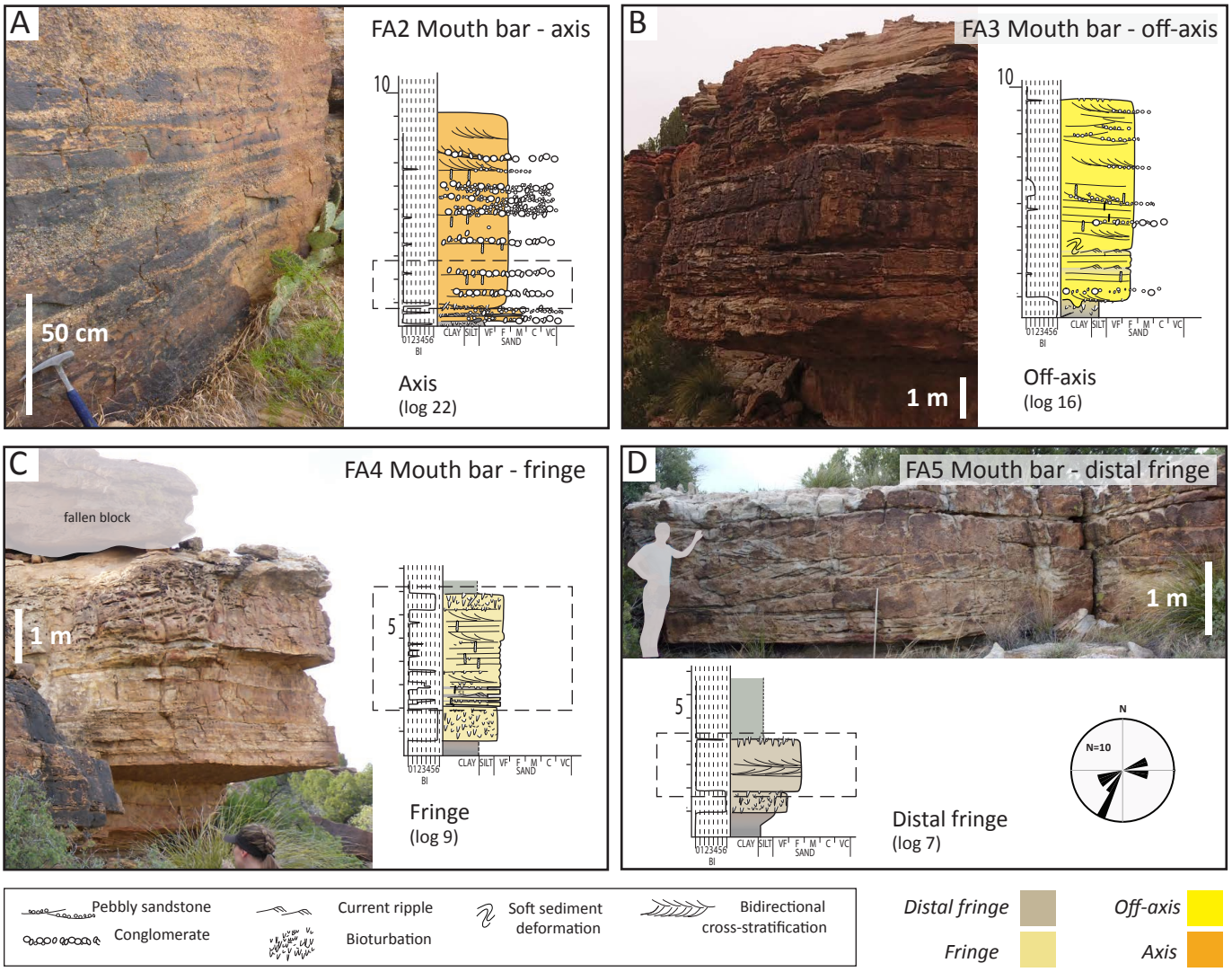
A
FA2 Mouth bar - axis
50 cm
10
CLAY SILT VF F M C VC
SAND
0123456
BI
Axis
(log 22)
B
FA3 Mouth bar - off-axis
1 m
10
CLAY SILT VF F M C VC
SAND
0123456
BI
Off-axis
(log 16)
C
FA4 Mouth bar - fringe
fallen block
1 m
5
CLAY SILT VF F M C VC
SAND
0123456
BI
Fringe
(log 9)
D
FA5 Mouth bar - distal fringe
1 m
5
CLAY SILT VF F M C VC
SAND
0123456
BI
N
N=10
Distal fringe
(log 7)
Pebbly sandstone
Conglomerate
Current ripple
Bioturbation
Soft sediment deformation
Bidirectional cross-stratification
Distal fringe
Fringe
Off-axis
Axis

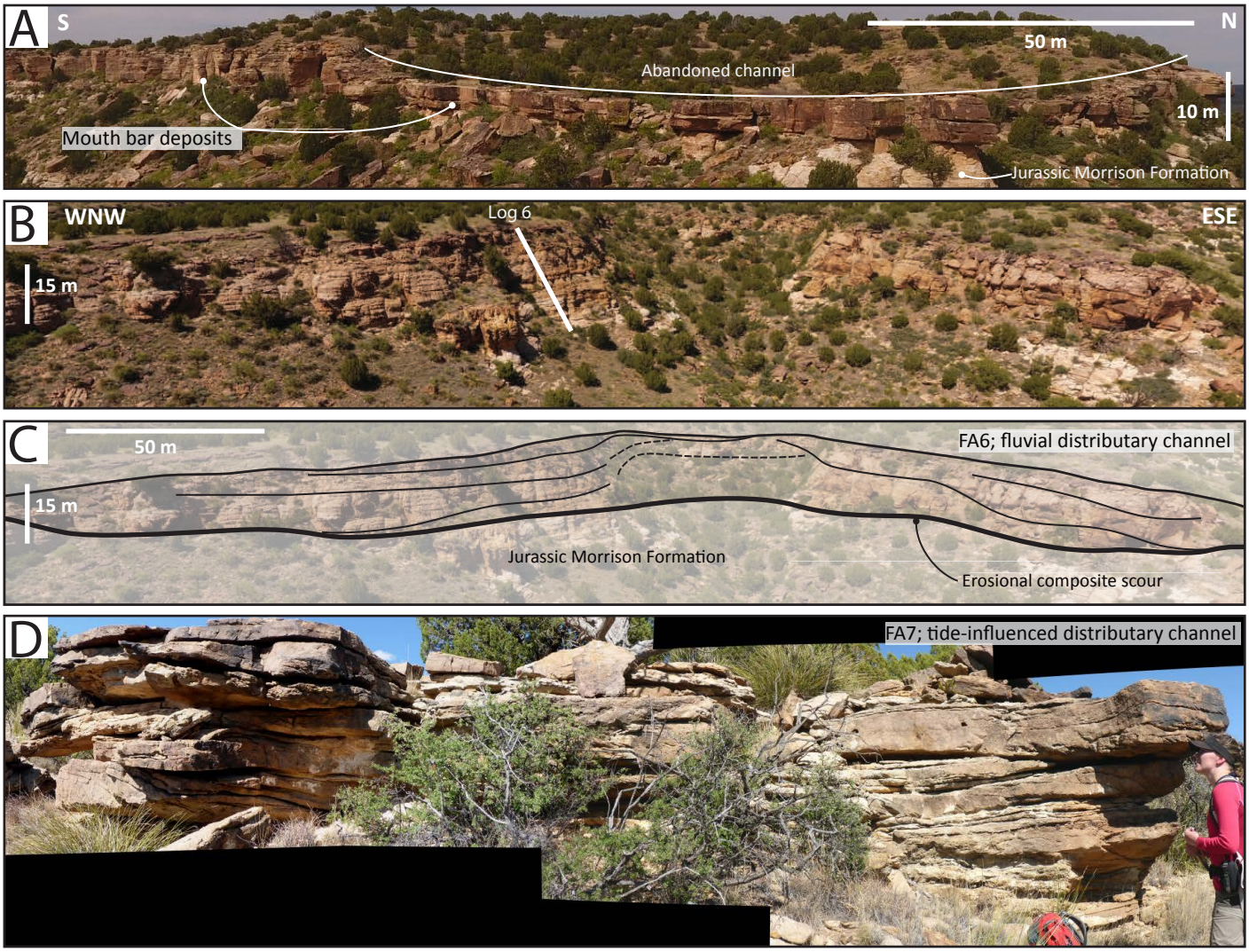
A
S
N
50 m
Abandoned channel
10 m
Mouth bar deposits
Jurassic Morrison Formation
B
WNW
Log 6
ESE
15 m
C
50 m
FA6; fluvial distributary channel
15 m
Jurassic Morrison Formation
Erosional composite scour
D
FA7; tide-influenced distributary channel

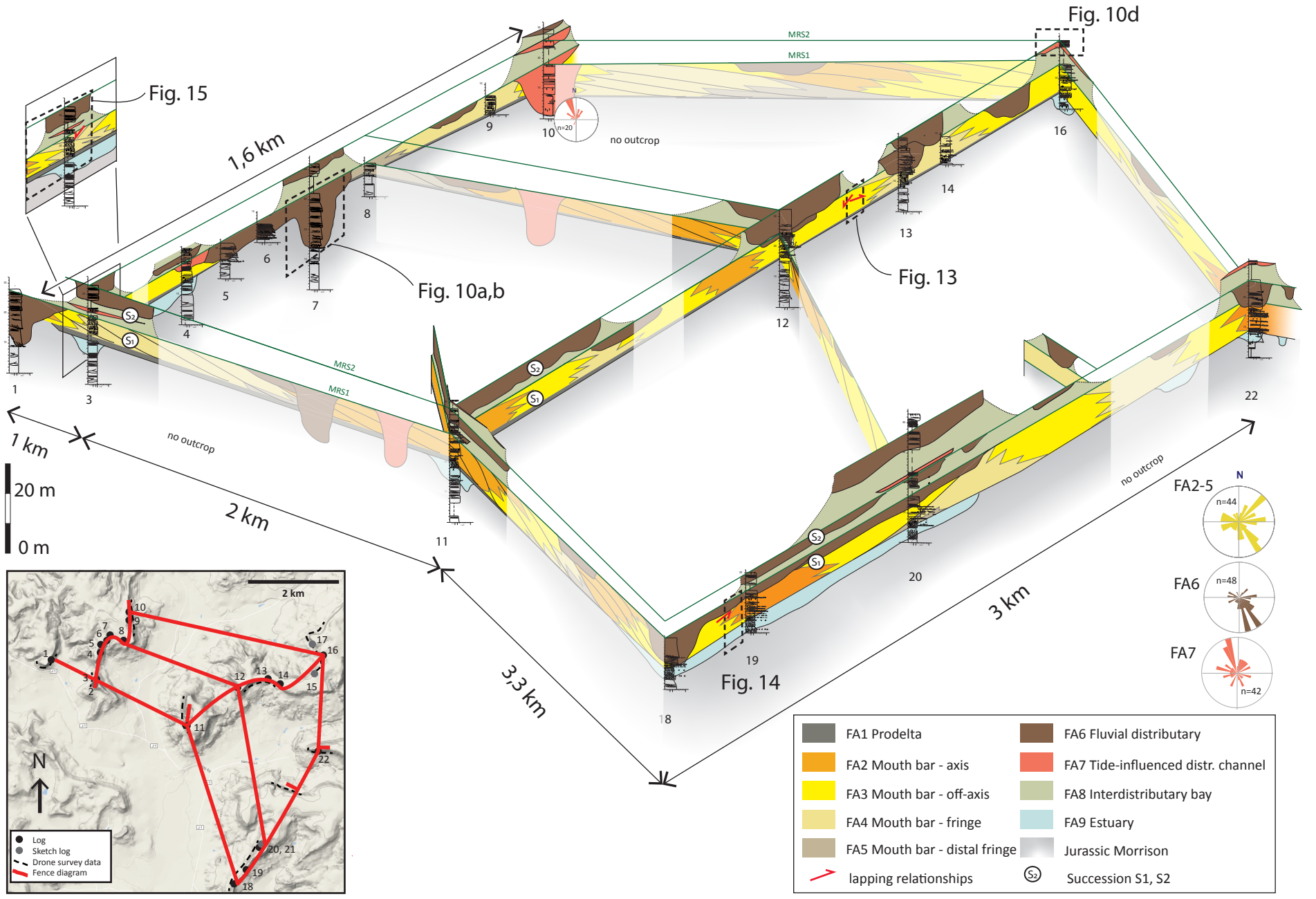
Fig. 15
Fig. 10d
Fig. 10a,b
Fig. 13
Fig. 14
MRS2
MRS1
no outcrop
1,6 km
1 km
2 km
3,3 km
3 km
20 m
0 m
S2
S1
FA2-5
FA6
FA7
n=44
n=48
n=42
n=20
FA1 Prodelta
FA2 Mouth bar - axis
FA3 Mouth bar - off-axis
FA4 Mouth bar - fringe
FA5 Mouth bar - distal fringe
FA6 Fluvial distributary
FA7 Tide-influenced distr. channel
FA8 Interdistributary bay
FA9 Estuary
Jurassic Morrison
lapping relationships
Succession S1, S2
2 km
Log
Sketch log
Drone survey data
Fence diagram

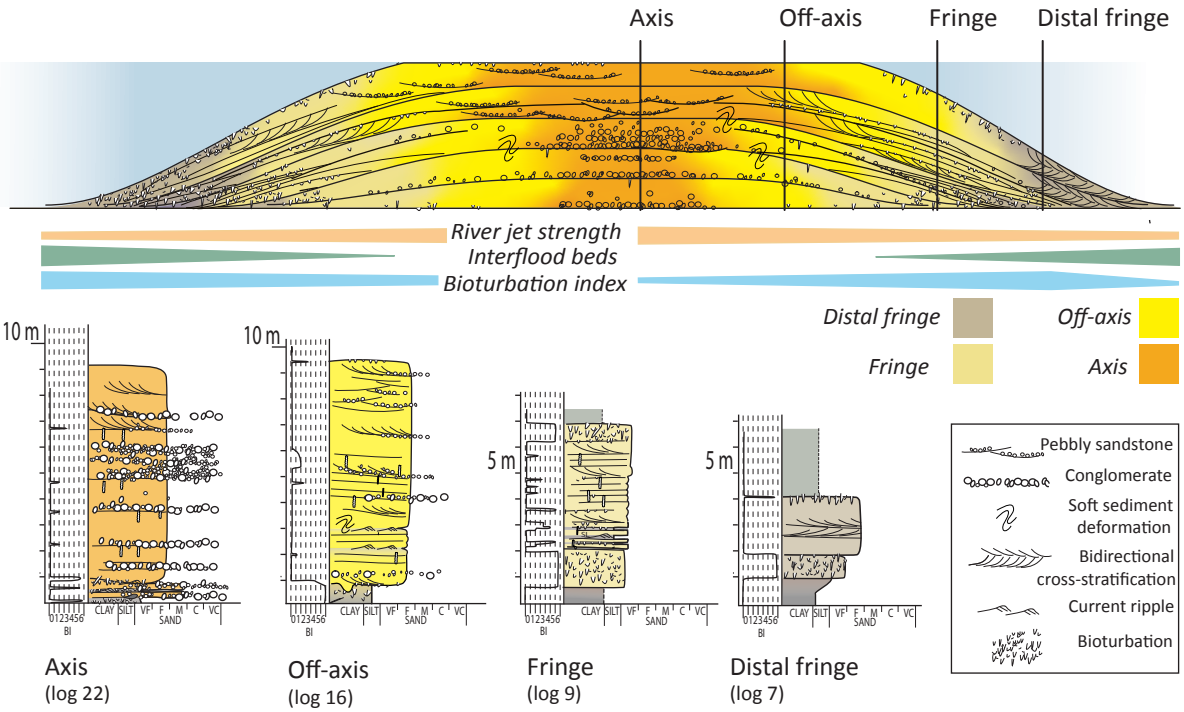

Axis
(log 22)

Off-axis
(log 16)

Fringe
(log 9)

Distal fringe
(log 7)

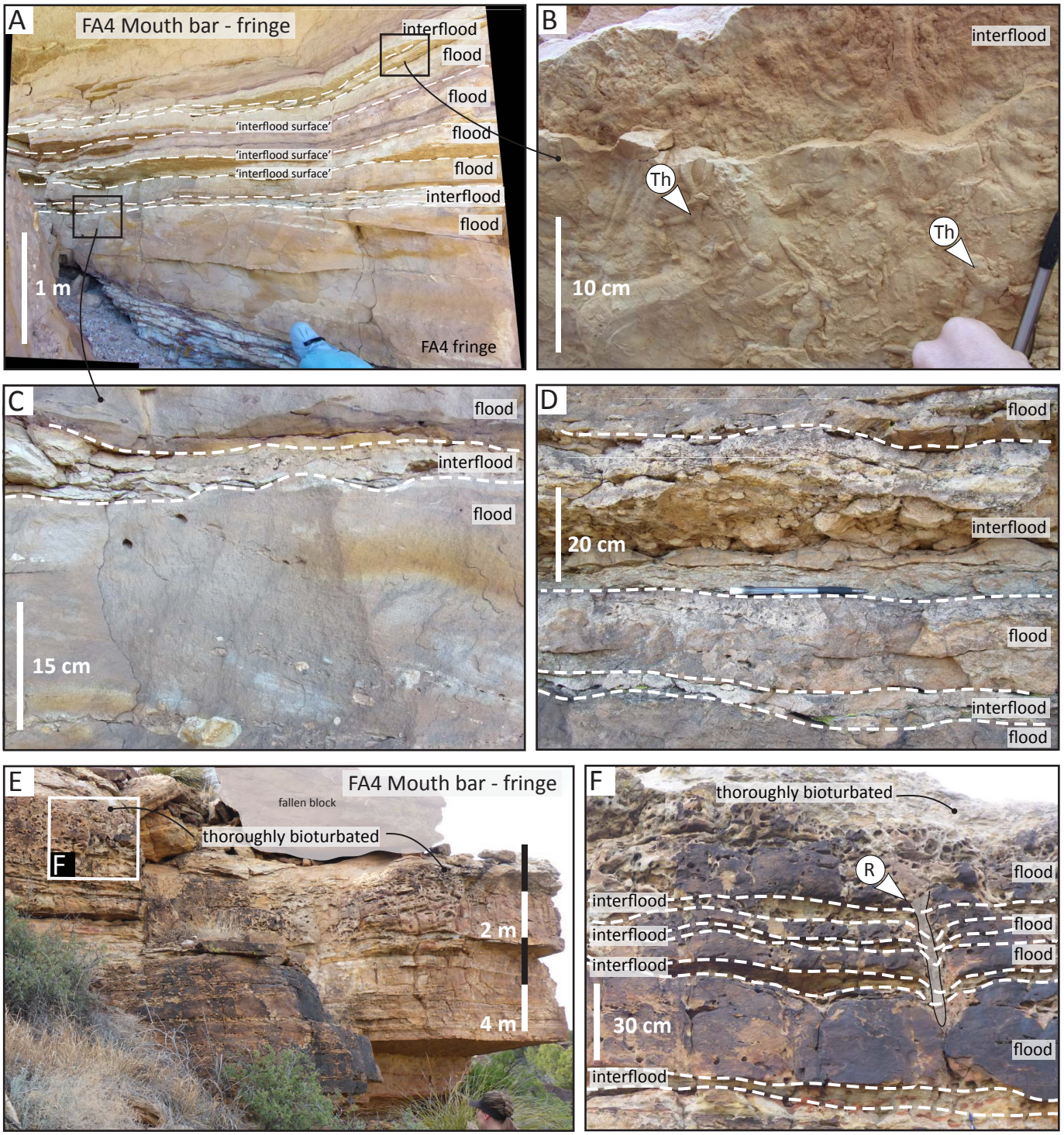
A
FA4 Mouth bar - fringe
interflood
flood
flood
'interflood surface'
flood
'interflood surface'
'interflood surface'
flood
interflood
flood
1 m
FA4 fringe
B
interflood
Th
Th
10 cm
C
flood
interflood
flood
15 cm
D
flood
interflood
20 cm
flood
interflood
flood
E
FA4 Mouth bar - fringe
fallen block
F
thoroughly bioturbated
2 m
4 m
F
thoroughly bioturbated
R
flood
interflood
flood
interflood
flood
interflood
30 cm
flood
interflood

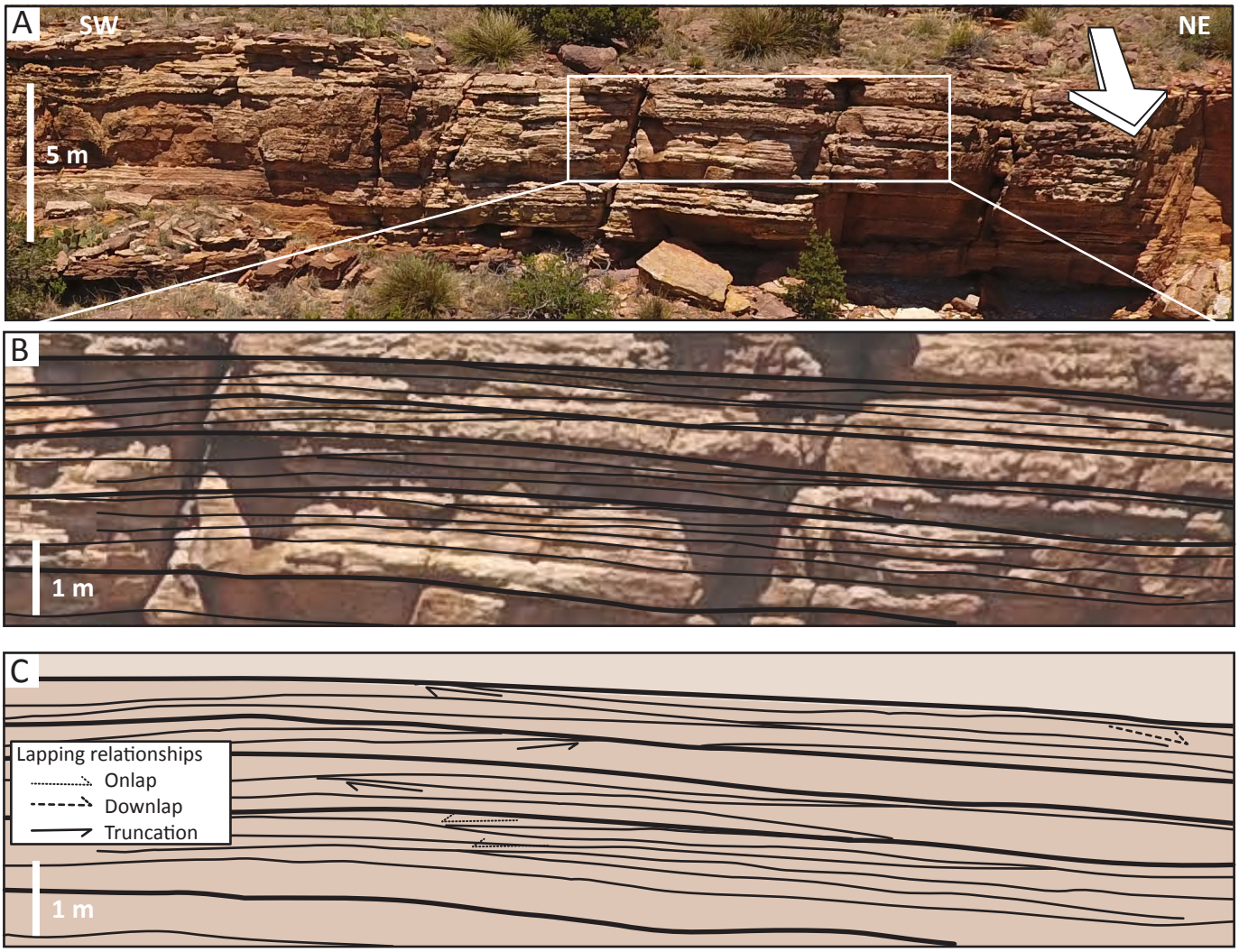
A
SW
NE
5 m
B
1 m
C
Lapping relationships
Onlap
Downlap
Truncation
1 m

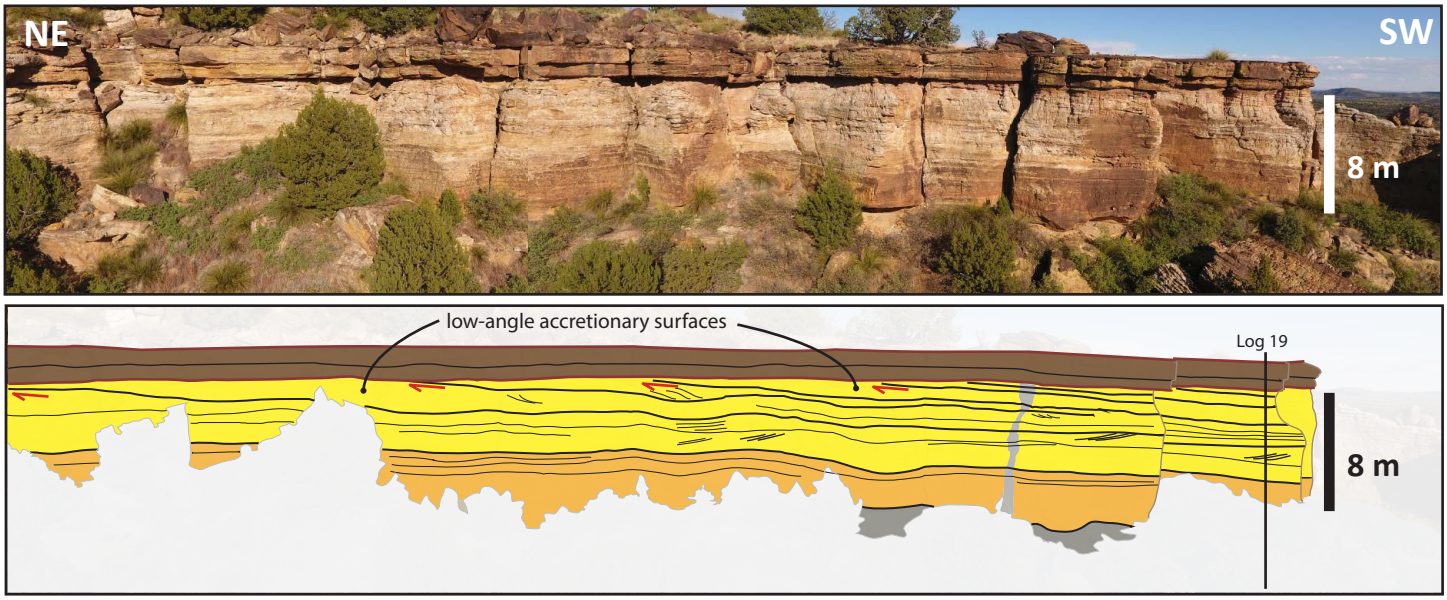
NE
SW
8 m
low-angle accretionary surfaces
Log 19
8 m
FA1 Prodelta
FA2 Mouth bar - axis
FA3 Mouth bar - off-axis
FA6 Fluvial distributary channel

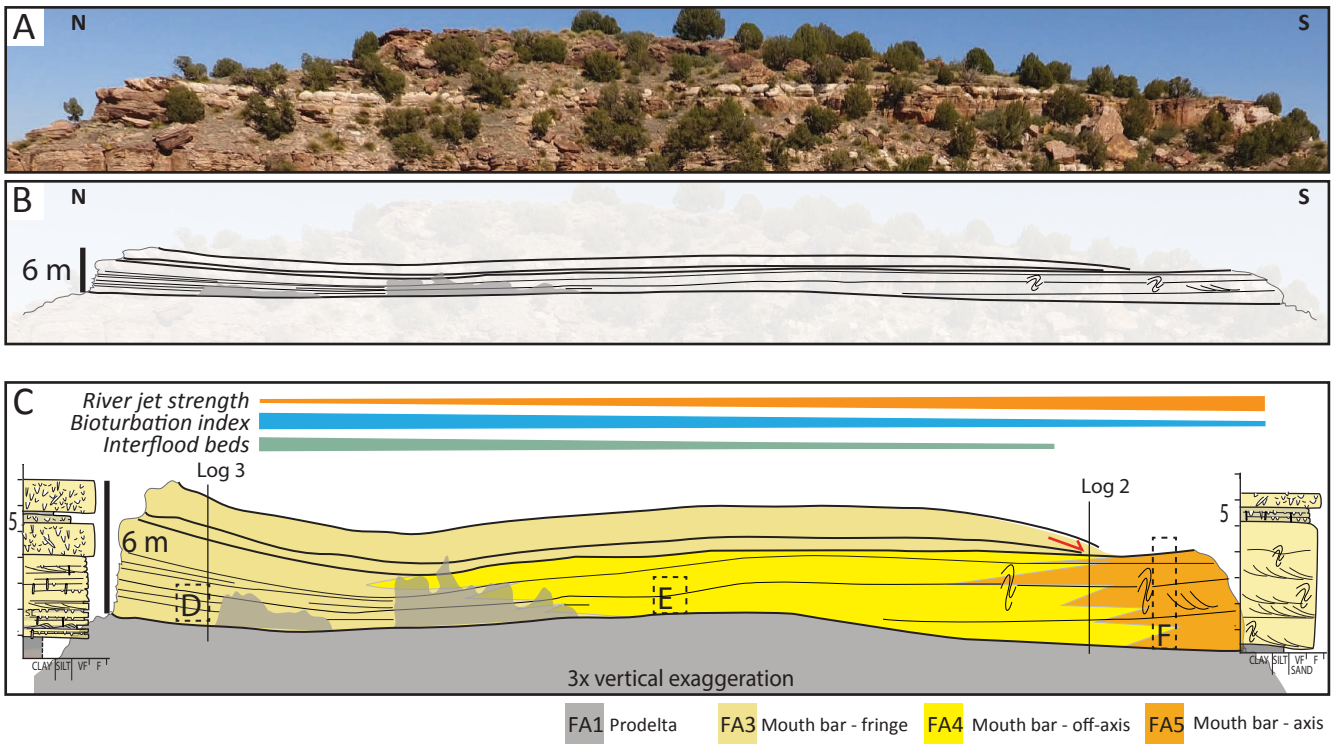
A
N
S
B
N
S
6 m
C
River jet strength
Bioturbation index
Interflood beds
Log 3
Log 2
6 m
D
E
F
5
5
CLAY SILT VF F
CLAY SILT VF F SAND
3x vertical exaggeration
FA1 Prodelta
FA3 Mouth bar - fringe
FA4 Mouth bar - off-axis
FA5 Mouth bar - axis

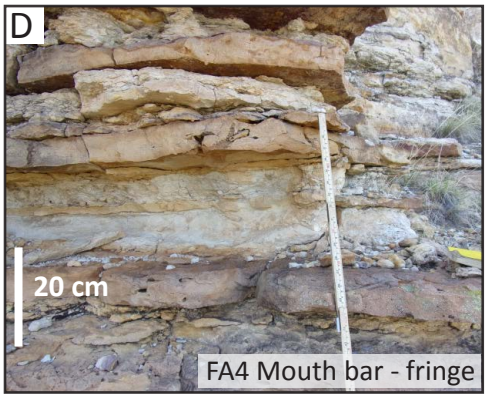
D
20 cm
FA4 Mouth bar - fringe


E
50 cm
FA3-4 Mouth bar - off-axis to fringe


F
1 m
FA2 Mouth bar - axis

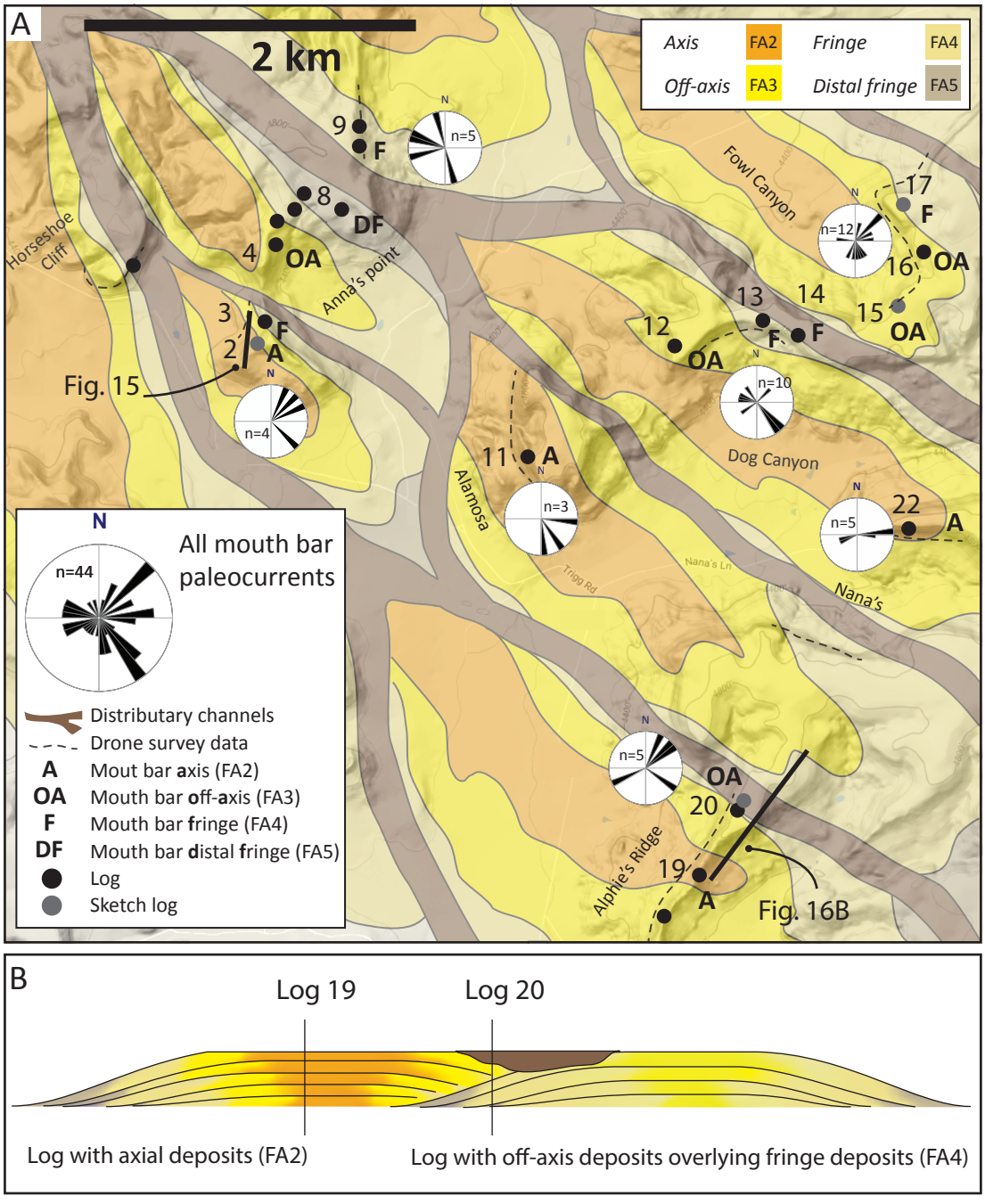
A
2 km
Axis
FA2
Fringe
FA4
Off-axis
FA3
Distal fringe
FA5
Horseshoe Cliff
Anna's point
Fowl Canyon
Dog Canyon
Alamosa
Trigg Rd
Nana's Ln
Nana's
Alphie's Ridge
Fig. 15
Fig. 16B
n=5
n=12
n=4
n=10
n=3
n=5
n=5
n=44
All mouth bar paleocurrents
Distributary channels
Drone survey data
A Mout bar axis (FA2)
OA Mouth bar off-axis (FA3)
F Mouth bar fringe (FA4)
DF Mouth bar distal fringe (FA5)
Log
Sketch log
B
Log 19
Log 20
Log with axial deposits (FA2)
Log with off-axis deposits overlying fringe deposits (FA4)

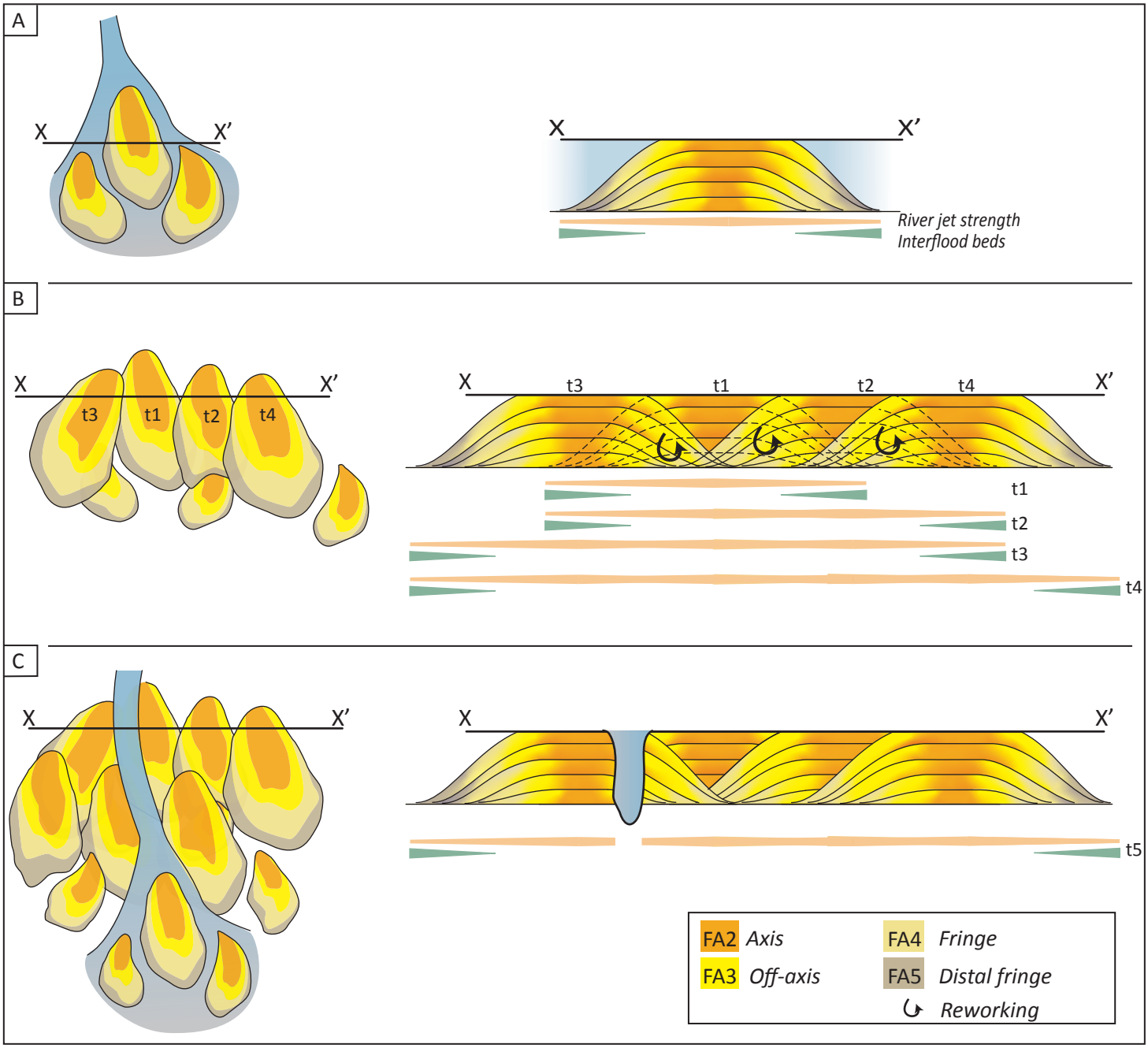
A
X
X'
X
X'
River jet strength
Interflood beds
B
X
t3
t1
t2
t4
X'
X
t3
t1
t2
t4
X'
t1
t2
t3
t4
C
X
X'
X
X'
t5
FA2 Axis
FA3 Off-axis
FA4 Fringe
FA5 Distal fringe
Reworking